의학박사 학위논문

뼈 발달과 재생에서 ARD1 라이신 아세틸화 효소의 억제 효과: 조골세포의 Runx2에 대한 억제성 되먹임 기전

Inhibitory roles of the lysyl-acetyltransferase ARD1 in bone development and regeneration: ARD1 controls osteoblast differentiation by inhibiting Runx2 in a feedback manner.

2014년 8월

서울대학교 대학원
의과학과 의과학전공 (약리학)
윤 혜 진

A thesis of the Degree of Doctor of Philosophy

Inhibitory roles of the lysyl-acetyltransferase ARD1 in bone development and regeneration: ARD1 controls osteoblast differentiation by inhibiting Runx2 in a feedback manner.

뼈 발달과 재생에서 ARD1 라이신 아세틸화 효소의 억제 효과: 조골세포의 Runx2에 대한 억제성 되먹임 기전

August 2014

The Department of Biomedical science
(Pharmacology),
Seoul National University
College of Medicine
Haejin Yoon

Inhibitory roles of the lysyl-acetyltransferase ARD1 in bone development and regeneration: ARD1 controls osteoblast differentiation by inhibiting Runx2 in a feedback manner.

by

Haejin Yoon

A thesis submitted to the Department of Biomedical science in partial fulfillment of the requirements for the Degree of Doctor of Philosophy in Biomedical science at Seoul National University College of Medicine

June 2014

Approved by Thesis Committee:

Professor _____Chairman

Professor _____Vice chairman

Professor _____

Professor _____

Professor _____

Inhibitory roles of the lysyl-acetyltransferase ARD1 in bone development and regeneration: ARD1 controls osteoblast differentiation by inhibiting Runx2 in a feedback manner.

뼈 발달과 재생에서 ARD1 라이신 아세틸화 효소의 억제 효과: 조골세포의 Runx2에 대한 억제성 되먹임 기전

지도 교수 박 종 완

이 논문을 의학박사 학위논문으로 제출함

2014년 06월

서울대학교 대학원
의과학과 의과학전공
윤 혜 진

윤혜진의 의학박사 학위논문을 인준함

위 원 장 _____ (인)
부위원장 _____ (인)
위 원 _____ (인)
위 원 _____ (인)
위 원 _____ (인)

ABSTRACT

Introduction: Runx2 has a pivotal role of bone formation and osteoblast differentiation. During an early stage of differentiation, Runx2 is upregulated and its activity is fine-tuned by post-translational modification. The lysyl-acetylation is an important modification to regulate Runx2 activity, and it has been known to be mediated by p300 or PCAF. However, which lysine residues in Runx2 are acetylated remains unclear so far. On the other hand, the acetyltransferase arrest defective-1 (ARD1) has been originally identified in Saccharomyces cerevisiae and known to be crucial for yeast growth and sporulation. In mammalian cells, ARD1 has been reported to acetylate the lysine residues of several proteins, such as, hypoxia-inducible factor-1α, β-catenin and myosin light chain kinase. As it is ubiquitously expressed, ARD1 is expected to act more diversely beyond the aforementioned functions. In the present study, it is investigated whether ARD1 participates in the Runx2 signaling pathway and bone formation.

Methods & Results: Both ARD1 and Runx2 were induced during bone morphogenic protein 2 (BMP-2) dependent osteoblastogenesis. In osteoblast differentiation, Runx2 suppressed IKKβ, which induces the proteasomal degradation of ARD1 by phosphorylating its S206, and by doing so stabilized ARD1. ARD1 inhibition increased osteoblastogenesis by activating Runx2, suggesting that ARD1 acts as a negative feedback regulator of Runx2. ARD1

knock-down augmented BMP-2-induced bone regeneration in rat calvarial defect model. Calvarial bone development at the neonatal stage was delayed in ARD1 transgenic mice. On the contrary, ARD1 knock-out promoted bone formation and mineralization in calvarias of newborn mince. In detailed mechanism, ARD1 was found to acetylate lysine 225 residue in the RUNT domain of Runx2, and this acetylation interfered with CBFβ binding to the RUNT domain of Runx2. Accordingly, ARD1 repressed the transcriptional activity of Runx2 and affected inhibition of Runx2-dependent osteoblast differentiation.

Conclusions: These results suggest that ARD1 acts as a guard that ensures balanced osteogenesis by fine-tuning Runx2 in a negative feedback manner. Taken together, this study shows that ARD1 has a new function in bone formation and should be considered a therapeutic target to aid bone healing.

– –

Keywords: osteoblast differentiation, ARD1, Runx2, BMP-2

Student number: 2011-30631

CONTENTS

LIST OF TABLES AND FIGURES

LIST OF TABLES AND FIGURES

LIST OF TABLES AND FIGURES

LIST OF ABBREVIATIONS

ALP, alkaline phosphatase

ARD1, arrest-defective 1

BMP, bone morphogenic protein

BSP, bone sialoprotein

CBFβ, core-binding factor β

CHX, cycloheximide

OCN, osteocalcin

OG2, osteocalcin gene 2

OSE, osteocalcin specific element

Runx2, RUNT-related transcription factor 2

INTRODUCTION

The bone is a dynamic tissue that continuously undergoes bone formation and remodeling. The bone microenvironment is composed of mineralized extracellular matrix and particular cell types, which are osteoblasts, osteoclasts, osteocytes. The osteoblasts, which take charge of bone formation, and the osteoclasts, which regulate bone resorption, work together in maturation and maintenance of the vertebrate skeleton by their balancing activities. Osteoblast cells are bone making cells and contain mesenchymal progenitors, preosteoblasts, mature osteoblasts, bone-lining cells and osteocytes (Long, 2012). Osteoblasts express many factors such as alkaline phosphatase, osteocalcin, osteopontin (known as bone sialoprotein-1) and type I collagen, and these factors cooperatively accumulate calcium phosphate in the form of hydroxyapatite to make bone hard (mineralization). At the end of process, the osteoblasts become inactive cells, which named as bone-lining cells, or undergo apoptosis. During these bone formation and remodeling, many transcription factors must be orchestrated. In particular, Runt-related transcription factor 2 (Runx2) leads the differentiation during the early phase (Schroeder et al., 2005).

Runx2 (also known as Cbfa1, PEBP2A1, and AML3) is expressed in mesenchymal stem cells, which is a key regulator in osteoblast differentiation and also participate in chondrocyte differentiation signaling. The Runx family,

which consists of Runx1, Runx2, and Runx3, has highly conserved the runt-homologous, DNA binding domain (Jonason et al., 2009; Blyth et al., 2005; Ito., 2004). The members of Runx family have proper expression in each organ and functions. Runx1 is essential for hematopoietic stem cell differentiation and is related to acute myeloid leukemia (Cameron et al., 2004; Okuda et al., 1996). Runx3 is necessary to regulate gastric epithelial cell growth and participated in gastric cancer (Li et al., 2002). Also, it involves in neurogenesis of the dorsal root ganglia (Levanon et al., 2002). Additionally, Runx3 cooperates with Runx2 and has an extra-function in chondrocyte proliferation and maturation in late stage (Sato et al., 2008). Runx2 has a major role in osteoblast differentiation (Choi et al., 2001; Komori., 2011). Runx2-deficient mice have lack of mature osteoblasts and, show decreased the expression levels of target genes such as alkaline phosphatase (ALP), bone sialoprotein-1 (BSP), and osteocalcin (OCN). The primary osteoblast cells which were derived from the calvarias of Runx2-deficient mice failed to differentiate to mature osteoblasts (Otto et al., 1997). Similarly, loss-of-function mutations in human Runx2 induce the cleidocranial dysplasia (CCD). CCD is a skeletal and dental disorder that shows hypoplastic clavicles, delayed closure of the fontanel, supernumerary teeth and short stature (Mundlos et al., 1997; Zhang et al., 2000).

Runx2 is classified type I and II. Type I is expressed mainly in pre-osteoblast and chondrocyte precursor cells, whereas type II is in mature osteoblasts and terminal hypertrophic chondrocytes (Park et al., 2001). Runx2

expression and function are controlled by multiple signaling pathways. During bone development, Runx2 are regulated by cytokines, growth factors, and hormones such as BMPs, TGF-β, FGF, sonichedgehog, and estrogen (Nishimura et al., 2012; Lee et al., 2000; Xiao et al., 2002; Komori., 2011). For instance, BMP-2, which is a member of the transforming growth factor‑β (TGFβ) superfamily, induces the transcriptional activation of Runx2. This action is processed by the BMP-2 binding to Ser/Thr kinase receptor and the activation of SMADs via receptor phosphorylation. To acquire transcriptional activity, Runx2 requires CBFβ (a non-DNA-binding partner), which allosterically enhances Runx2 binding to DNA (Schroeder et al., 2005; Franceschi et al., 2007). The Runx2-CBFβ complex binds to a conserved nucleotide sequence (R/TACCRCA), and turns on the expressions of several osteogenic proteins, such as, collagen α1, osteopontin, BSP, and OCN (Ducy et al., 1997; Komori., 2010).

During osteoblast differentiation, Runx2 is up-regulated at the protein level and activated functionally, which is modulated by the post-translational modification. This post-translational modification of Runx2 shows two-faced function. Runx2 is activated by phosphorylation of its serine or threonine residues through the MAPK-ERK pathway, which is stimulated by fibroblast growth (Komori., 2011; Long et al., 2012). However, the phosphorylation of serine 104 and serine 451 residue of Runx2 inhibit the interaction of Runx2 with CBFβ and decrease its transcriptional activity (Wee et al., 2002).

Furthermore, when Runx2 is phosphorylated at other serine residues by GSK3β and CDK4, it becomes destabilized and repressed functionally (Jonason et al., 2009). Those studies have demonstrated that Runx2 protein undergoes degradation by ubiquitin-dependent manner (Bae et al., 2006). For instance, Hect domain E3 ligase (WWP1), Schnurri-3 (Shn3) and C terminus of Hsc70-interacting protein (CHIP) regulate the ubiquitination and degradation of Runx2. In addition, acetylation is involved in the Runx2 signaling pathway. Acetylation at histone lysine residues reorganizes the chromatin structure to induce Runx2-dependent gene expression (Sierra et al., 2003; Chan et al., 2001). Furthermore, Runx2 can be lysyl-acetylated directly by some acetyl-transferases. For instance, p300 and p300/CBP-associated factor (PCAF) have been reported to acetylate Runx2 at lysine residues and to enhance the transcriptional activity (Jeon et al., 2006). While the acetylation of Runx2 through p300 is well-known, the target site of Runx2 is unclear. Likewise, monocytic leukemia zinc finger protein (MOZ) and MOZ-related factor (MORF) which known as the acetyl-transferases have been reported to activate Runx2, but it is uncertain whether they directly acetylate Runx2 (Pelletier et al., 2002). While acetylation of Runx2 has been studied for a long time, the precise regulation of Runx2 has been unclear.

Acetylation is a common post-translational protein modification in eukaryotes. Acetylation classifies two patterns, N-terminal α-acetylation and lysine ε-acetylation. N(α)-acetylation is an enzymatic reaction that acts on the α-amino group of the N-terminal amino acid (Polevoda et al., 2003). Most of

mammalian proteins are acetylated at their N-termini during translation, and N(α)-acetylation is required for the regulation of protein–protein interactions, functions and stabilities. The lysine ε-acetylation is the enzymatic reaction that acts on the ε-amino group of the lysine residue at the post-translational level. The ε-acetylation regulates many diverse functions of proteins such as DNA recognition, protein–protein interactions, and protein stability (Kouzarides., 2000).

The acetyl-transferase arrest defective-1 (ARD1), which is officially referred to as N-α-acetyltransferase 10 (also called NAA10, ARD1A, DXS707, and TE2), was first identified in Saccharomyces cerevisiae and has been found to be crucial for yeast growth and sporulation (Whiteway et al., 1985). ARD1 and NAA15 are component of N-terminal acetyltransferase (NAT) complex (Arnesen et al., 2005). ARD1 acts as a catalytic subunit in the NAT complex (Liszczak et al. 2013). Its orthologs have been identified in mouse and human cells, and participate in cell growth and proliferation, as shown in yeasts (Arnesen., 2009). ARD1 has various isoforms which show conserved N-acetyltransferase domain in mouse such as $mARD1^{198}$, $mARD1^{225}$, and $mARD1^{235}$, and in human such as $hARD1^{131}$ and $hARD1^{235}$. Despite of similar structure, ARD1 isoforms have their specific roles in different cells. For example, mouse $ARD1^{225}$ induces HIF-1α acetylation and degradation, but other forms of ARD1 have no such effect (Fisher et al., 2005; Jeong et al., 2002).

Functionally, ARD1 catalyzes the N-terminal α-acetylation of proteins in yeast and mammalian cells (Mullen et al., 1989; Fisher et al., 2005), and it is also known to induce the lysine ε-acetylation of several proteins, including hypoxia-inducible factor-1α, β-catenin, myosin light chain kinase, and androgen receptor (Jeong et al., 2002; Lim et al., 2006; Shin et al., 2009; Wang et al., 2012). ARD1 has several functional domains including acetylase domain and nuclear localization signal (NLS) among amino acids 78–83 (KRSHRR). NLS changes the location from cytosol to nucleus of ARD1, which is expressed in both the nucleus and cytoplasm in various cell types (Arnesen et al., 2005). Because ARD1 is ubiquitously expressed in many human cells, it is expected to have diverse functions including cell cycle regulation. For instance, by leading lysyl acetylation of β-catenin, ARD1 upregulates cyclin D1 and promotes lung cancer cell proliferation (Lim et al., 2006). Although ARD1 has an oncogenic role in tumor, ARD1 inhibits cell growth and activates autophagy by inhibiting mTOR signaling in breast cancer (Kuo et al., 2010). ARD1 induces RNA expression of Beclin 1, which is a mammalian autophagy gene, through mTOR signaling. ARD1 affects DNA damage-induced caspase activation and apoptosis. Thus, ARD1 shows opposite functions in different conditions and is still controversial. In addition, ARD1 is related to neuronal dendritic development and prevent Alzheimer's disease through suppression of the Aβ secretion (Ohkawa et al., 2008; Sugiura et al., 2003). Therefore, the investigation of ARD1's actions helps understand cell physiology.

In a view point of ARD1 regulation, ARD1 is controlled by three types of signaling. First, ARD1 is decreased under hypoxic conditions (Jeong et al., 2002; Fisher et al., 2005), but this mechanism is controversial in different cell types. Second, ARD1 is cleavaged caspase-dependent during the apoptosis (Arnesen et al., 2005). Finally, ARD1 is phosphorylated at serine 206 residue by IκB kinase β (IKKβ), and it becomes to undergo proteasome-mediated degradation (Kuo et al., 2009).

Summarizing, ARD1 is believed as an all-around player in cell signaling. ARD1 acetylates various proteins involved in multiple cellular functions including apoptosis, cell proliferation, metabolism, and cell-cell interaction. However, no study has addressed the role of ARD1 in bone formation. To examine if ARD1 participates in bone formation, I firstly expected that ARD1 regulates the Runx2-driven osteoblast differentiation because Runx2 is a key regulator on the osteogenesis. In this study, I tested this possibility *in vitro* and *in vivo*.

MATERIALS AND METHODS

Preparation of plasmids, siRNAs and transfection.

Myc-tagged mouse Runx2 plasmid and 6xOSE/OG2 reporter plasmids were kindly given by Dr. Hyun-Mo Ryoo (Seoul National University School of Dentistry). Human CBFβ cDNA was cloned using RT-PCR and inserted into the Myc-tagged pcDNA. The plasmids for Flag/SBP-tagged Runx2 fragments were re-cloned from the mouse Runx2 plasmid using PCR and blunt-end ligation. Site-specific mutations of Runx2 were performed using PCR-based mutagenesis (Stratagene; Cedar Creek, TX). The ARD1 plasmid was constructed as previously described (Lim et al., 2006). For transient transfection with plasmids or siRNAs, cells at ~40% density were transfected with plasmids or siRNAs using calcium phosphate or Lipofectamine reagent (Invitrogen). The transfected cells were allowed to be stabilized for 48 hours before being used in experiments. The shRNAs containing a hairpin loop were synthesized and inserted into pLKO.1-puro vector. The viral vectors were co-transfected into HEK293T cells with pRSV-Rev, pMD2-VSVG, and pMDLg/pRRE plasmids to prepare viral particles. On the 3rd day after transfection, Lenti viruses were collected from the supernatant of HEK293T cells. C2C12 cells were infected with viruses (100 μl/ml) and selected using puromycin (2 μg/ml) to establish stable cell lines.

Reagents and antibodies.

Culture media were purchased from Invitrogen (Carlsbad, CA), and fetal calf serum from Sigma-Aldrich (St. Louis, MO. Recombinant human BMP-2 (bone morphogenic protein 2) was purchased from Perprotech (Rocky Hill, NJ). A polyclonal antibody against ARD1 was raised in rats against full-length human ARD1 (Lim et al., 2006). Mouse ARD1 and β-tubulin primary antibodies and HRP-conjugated secondary antibodies were purchased from SantaCruz Biotechnology (Santa Cruz, CA); anti-Runx2 from MBL (Nagoya, Japan); Acetylated-Lysine antibody from Cell Signaling Technologies (Billerical, MA); anti-α-Myc-tag and Flag-tag antibody from Sigma-Aldrich.

Isolation and culture of mouse primary osteoblasts

Calvarias of newborn mice were washed in HBSS (Life Technologies, NY) containing 3% penicillin and streptomycin. Isolated calvarias were sequentially digested in α-MEM containing 0.1% collagenase (Sigma-Aldrich) and 0.2% Dispase II (Roche, Switzerland) at 37℃. Digestion was carried out five times (for 30 minutes per each digestion), and the fractions were pooled. Osteoblasts were collected by centrifugation and resuspended in ascorbic acid-free α-MEM. Osteoblasts were plated at 100-mm culture dishes and the media were replaced 24 hours later. To induce differentiation, cells were treated with ascorbic acid (50 μg/ml), β-glycerophosphate (2 mM) and BMP-2 (100 ng/ml). This procedure was approved by the Institutional Animal Care and Use Committee of Seoul National University (Approve # SNU-

120313-10-1).

Cell culture

C2C12 (mouse mesenchymal precursor), MC3T3-E1 (mouse pre-osteoblast) and HEK293T (human embryonic kidney) cell-lines were obtained from American Type Culture Collection (ATCC; Manassas, VA). Cells were cultured at 5% CO_2 in Dulbecco's modified Eagle's medium, supplemented with 10% heat-inactivated fetal bovine serum. C2C12 differentiation toward osteoblast was induced by BMP-2 (100 ng/ml) or Wnt3a (50 ng/ml). ATDC5 cell line (mouse chondrocyte), which was a kind gift from Dr. Dae-Won Kim (Yonsei University, Korea), was cultured at 5% CO_2 in 1:1 mixture of DMEM and Ham's F-12 medium containing 10% FBS. ATDC5 differentiation was induced by Insulin-Transferrin-Selenium Supplement (Life Technologies, NY) and BMP-2 (10 ng/ml).

Critical-size calvarial defects in rats

Male Spraque-Dawley rats (10 weeks old) were purchased from Orient Bio Inc (Gyeonggi-do, Korea) and kept in specific pathogen-free rooms. General anesthesia was induced using Zoletil and Rumpun. After a midline incision of the scalp, an 8 mm critically sized calvarial defect was created using a trephine bur (GEBR; Brasseler, Germany) under sterile saline irrigation. The calvaria was covered with a 1% collagen matrix (Bioland; Cheongwon, Korea) containing BMP-2 (1 mg) and shCon or shARD1 (5.0×10^9/ml), and

skin flaps were sutured. Six rats per each group were sacrificed 6 weeks after surgery. The calvarias were decalcified with 10% EDTA solution for 2 weeks and dehydrated through a series of ethanol solutions of increasing concentration and embedded in paraffin. The calvarial slices (5 μm thickness) were sectioned coronally at the center of defect, stained with hematoxylin and eosin (H&E), and subjected to immunohistochemistry. The procedures used and the care of animals were in accordance with the guide included in the Seoul National University Laboratory Animal Maintenance Manual (approve # SNU-111111-3).

ARD1 transgenic mice and ARD1 knock-out mice

Transgenic mice overexpressing mARD1[235] (mouse orthologue of human ARD1) were kindly given by Dr. Goo Taeg Oh (Ewha Women's University). Two different founders (#10 and #15) were bred in the hemizygous state, and transgenic and non-transgenic littermates were assigned into pair-matched groups for all experiments. Mice were fed a chow diet and water ad libitum in the Ewha Laboratory Animal Genomics Center under specific pathogen-free conditions. Wild-type and ARD1 transgenic mice were sacrificed on postnatal day 3 to examine the extent of bone development. After the skulls were carefully isolated from skin and brain, they were washed with PBS and fixed in 10% formalin for 24 hours. All experiments were approved by the Institutional Animal Care and Use Committees (IACUC) of Ewha Women's University, and adhered to the National Research Council Guidelines (approve

2010-24-2).

Also, ARD1 knock-out mice were given by Dr. Goo Taeg Oh (Ewha Women's University). All experiments were performed according to the protocol approved by the Institutional Animal Care and Use Committees (IACUC) of Ewha Women's University.

Alkaline Phosphatase, Alizalin Red S, and von Kossa stainings.

C2C12 cells were cultured on 6-well plates at a density of $1x10^5$ cells/well, and ALP was visualized using naphthol AS-MX phosphate (Sigma-Aldrich) as a substrate. After being differentiated by BMP-2, cells were fixed with 10% formaldehyde for 5 minutes, briefly rinsed by water, and permeabilized by 0.1 % Triton X-100. Cells were incubated at 37℃ for 30 minutes in a mixture containing sodium nitrite, FRV-Alkaline solution (Sigma-Aldrich) and Naphthol-AS-BL alkaline solution (Sigma-Aldrich). After being rinsed by water, wells were photographed. The calcification of osteoblast was analyzed by Alizarin Red staining. After fixed in 10% formaldehyde and washed with distilled water, cells were stained with 1% Alizarin Red S at room temperature for 20 minutes. Wells were rinsed with water and photographed. Mineralization of bone tissues was evaluated by von Kossa staining. Rat calvarias were fixed with 3.7% paraformaldehyde and embedded in epoxy resin. Calvarial sections were incubated with 1% silver nitrate and exposed to bright light for 30 minutes. After silver was removed by 5% sodium thiosulfate, sections were counterstained with Nuclear Fast Red.

Histological procedure

Bone tissues were decalcified with 10% EDTA solution for 2 weeks and dehydrated through a series of ethanol solutions of increasing concentration and embedded in paraffin. The calvarial slices (5 μm thickness) sectioned coronally at the center of defect was stained with hematoxylin and eosin (H&E).

Alcian blue/Alizarin red co-staining of skeletons

After the skin and internal organs were removed, mice were fixed in ethanol for 5 days. Mice were stained with 0.015% Alcian Blue 8GX and 0.005% Alizarin Red S in ethanol/acetic acid (9:1. v/v) at 37 ℃ for 48 hours. After being rinsed with water, skeletons were kept in 1% KOH solution with 20% glycerol until they became clearly visible.

Quantitative microcomputed tomography (micro-CT)

Calvarial bones were removed and fixed in 10% formalin, and micro-CT was taken using NFR Polaris-G90 manufactured by Nanofocusray (Jeonju, Korea). The scanner uses an X-ray source and has a camera that rotates around a bed holding the samples. The samples were scanned at a tube potential of 65 kVp and a tube current of 120 μA for 15 minutes. Data were acquired from the 1024 images of reconstruction with an isotropic voxel spacing of 0.034 × 0.034 × 0.027 mm^3. The volume of bone ingrown in a defect site was

analyzed by the three-dimensional analysis using a software Amira version 5.4.1 (San Diego, CA). The bone range was reflected with CT analyzer manual which was ranged more than 1000 CT number, and the CT number of air (1000 HU) and water (0 HU) was used to calibrate the image values in Hounsfield units. To distinguish bone tissue from soft tissue, the CT number was given a range of brain and cortical-bone equivalent hydroxyapatite material. The mean value was determined by CT number.

Sequences of siRNAs and shRNAs

The sequences of siRNAs used were 5'-CCAACACCCTCAACTTTCAGATCAG-3' for silencing mouse ARD1 and 5'-AUGAACGUGAAUUGCUCAATT-3' for non-targeting control. The sequences of ARD1 shRNAs are 5'-CCGGCCGGAGAACTACCAGATGAAGCTCGAGCTTCATCTGGTAGTTCTCCGGTTTTT-3' for mouse sh ARD1-I, 5'-CCGGACACCCTCAACTTTCAGATCACTCGAGTGATCT GAAAGTTGAGGGTGTTTTTT-3' for mouse sh ARD1-II and rat shARD1, and 5'-CCGGTACAACAGCCACAACGTCTATCTCGAGATAGACGTTGTGGCTGTTGTATTTTT-3' for non-targeting shRNA.

Semi-quantitative RT-PCR

The mRNA levels were quantified using a highly sensitive semi-quantitative RT-PCR. Total RNAs were extracted using TRIZOL (Invitrogen) and reverse-transcribed at 46 ℃ for 20 min. The cDNAs were amplified over 17 PCR cycles with 5 μCi [α-^{32}P]dCTP. The PCR products were electrophoresed on a

4% polyacrylamide gel, and the dried gel was autoradiographed. PCR primer sequences are 5'-AACCTCAAAGGCTTCTTCTT-3' and 5'-ACATGGGGAATGTAGTTCTG-3' for mouse ALP and 5'-AAGAGAGGCATCCTCACCCT-3' and 5'-ATCTCTTGCTCGAAGTCCAG-3' for mouse β-actin.

RT-qPCR

Total RNAs were extracted using TRIZOL (Invitrogen), and reverse-transcribed in a reaction mixture containing M-MLV Reverse Transcriptase (Promega; Madison, WI), RNase inhibitor, dNTP, and random primers at 46 ℃ for 30 min. Quantitative real-time PCR on 96-well optical plates was performed in the Evagreen qPCR Mastermix, and fluorescence emitting from dye-DNA complex was monitored in CFX Connect Real-Time Cycler (BIO-RAD). The levels of mRNAs were normalized by 18S RNA levels and represented as relative values. The primer sequences are 5'-GCAATAAGGTAGTGAACAGACTCC-3' and 5'-GTTTGTAGGCGGTCTTCAAGC-3' for mouse osteocalcin; 5'-AAGCAGCACCGTTGAGTATGG-3' and 5'-CCTTGTAGTAGCTGTATTCGTCCTC-3' for mouse bone sialoprotein; 5'-AACCTCAAAGGCTTCTTCTT-3' and 5'-ACATGGGGAATGTAGTTCTG-3' for mouse alkaline phosphatase; 5'-AACTTCTGTGGGAGCGACAA-3' and 5'-GGGAGGGAAAACAGAGAACGA-3' for mouse sex determining region Y-box 9 (Sox9).

Reporter assays.

Cells were co-transfected with 6xOSE-luciferase or OG2-luciferase and

CMV-β-gal using calcium phosphate or Lipofectamine reagent. The final DNA or siRNA concentration was adjusted by adding pcDNA or control siRNA, respectively. After 16 hours of stabilization, transfected cells were seeded on 4 dishes at a cell density of 5×10^4 cells/cm^2 and further cultured for 24 hours. The cells were incubated under normoxic or BMP-2 treated conditions for 48 hours, and then lysed to determine luciferase. β-gal activities were measured to normalize transfection efficiency.

Immunoblotting and immunoprecipitation.

Cell lysates were separated on SDS-polyacrylamide (8-12%) gels, and transferred to an Immobilon-P membrane (Millipore, Bedford, MA). Membranes were blocked with a Tris/saline solution containing 5% skim milk and 0.1% Tween-20 for 1 hour and then incubated overnight at 4℃ with a primary antibody diluted 1:1000 in the blocking solution. Membranes were incubated with a horseradish peroxidase–conjugated secondary antibody (1:5000) for 1 hour at RT, and stained using the ECL-plus kit (Amersham Biosciences, Piscataway, NJ). To analyze protein interactions, cell lysates were incubated with anti-Runx2, anti-Myc or anti-Flag antibody overnight at 4℃, and the immune complexes were pulled down by protein A/G beads (Santa Cruz, CA). The bound proteins were eluted in a denaturing SDS sample buffer or by Myc/Flag peptides, loaded on SDS-PAGE, and immunoblotted with anti-Runx2, anti-ARD1, anti-Myc, or anti–Flag antibody.

Chromatin immunoprecipitation (ChIP)

Cells were fixed with 1% formaldehyde for 10 minutes to crosslink chromatin complexes, and treated with 150 mM glycine to stop the crosslinking reaction. After cells were lysed and sonicated, soluble chromatin complexes were precipitated with anti-Runx2 antibody overnight at 4℃. DNAs were isolated from the precipitates and the precipitated DNA segment of the osteocalcin promoter was quantified by real-time PCR using the Evagreen qPCR Mastermix (Applied Biological Materials Inc; Richmond, Canada) in the CFX Connect™ Real-Time System (BIO-RAD). The ChIP-DNAs were amplified over 40 PCR cycles (95℃-53℃-70℃, 20 seconds at each temperature) and the DNA amplification was continuously monitored. The primer sequences used for qPCR amplifying the osteocalcin gene are 5'-TGCATAGGGTTCTTGTCTCT-3' and 5'-CTCCACCACTCCTACTGTGT-3'.

Alkaline Phosphatase (ALP) Activity.

The cultures were rinsed twice with ice-cold phosphate-buffered saline, solubilized in a lysis buffer (pH = 10.5, 50 mM Tris, 100 mM glycine, and 0.1% Triton X-100), and sonicated twice on ice for 15 seconds. The supernatant was collected and used to determine total protein and alkaline phosphatase (ALP) levels. Total protein levels were calculated using a BCA protein assay kit (Bio-Rad; Hercules, CA). A 100 μl aliquot of freshly prepared p-nitrophenyl-phosphate tablet solution was added to 200 μl of the supernatant samples and incubated at 37℃ for 30 minutes. The optical

density of p-nitrophenol was measured at 405 nm, and ALP activity was standardized as nmoles of p-nitrophenol per mg of protein per minute.

Preparation of cytosolic and nuclear extracts

Cells were centrifuged at 1,000xg for 5 minutes, and resuspended with a lysis buffer containing 10 mM Tris/HCl (pH 7.4), 10 mM KCl, 1 mM EDTA, 1.5 mM $MgCl_2$, 0.2% NP40, 0.5 mM dithiotheritol, 1 mM sodium orthovanadate, and 400 μM PMSF. The cell lysates were separated into pellet (for nuclear fraction) and supernatant (for cytosolic faction) using centrifugation at 1,000xg for 5 minutes. One packed volume of a nuclear extraction buffer (20 mM Tris/HCl, pH 7.4, 420 mM NaCl, 1 mM EDTA, 1.5 mM $MgCl_2$, 20% glycerol, 0.5 mM dithiotheritol, 1mM sodium orthovanadate, and 400 μM PMSF) was added to the pellet, and vortexed intermittently at low speed on ice for 30 minutes. The nuclear extracts were cleaned at 20,000xg for 10 minutes, and stored at -70^{o}C.

***In vitro* acetylation assay**

GST-tagged Runt domain, its K225R mutant or His-tagged ARD1 peptide was expressed in E. coli using IPTG, and then purified using GSH- or nickel-affinity beads. Recombinant His-ARD1 (0.5 μg) and GST-Runt (0.5 μg) peptides were incubated in a reaction mixture (50 mM Tris/HCl pH 8.0, 0.1 mM EDTA, 1 mM DTT, 10 mM sodium butyrate, 20 mM acetyl-CoA, and

10% glycerol) at 37℃ for 4 hours. Acetylated Runt peptides were identified by Western blotting using anti-acetyl-lysine antibody. To verify the presence of peptides, the mixture was run on a SDS-polyacrylamide gel and stained with 0.1% coomassie Brilliant Blue R-250, followed by being destained with 50% methanol and 10% glacial acetic acid.

In-Gel Digestion and Mass Spectrometric analysis.

After F/S-Runt peptide was co-expressed with *ARD1* in C2C12, the peptide was separated by a SDS-PAGE, digested in the gel slice with trypsin, and subjected to a nanoflow ultra-performance liquid chromatography/ESI/MS/MS with a mass spectrometer (Q-tof Ultra global), comprising a three-pumping Waters nano-LC system, a stream selection module, and MassLynx 4.0 controller (Waters, UK). Five μl of mixed peptides was dissolved in buffer C (water/acrylonitrile/formic acid; 95:5:0.2, V:V:V), injected on a column, and eluted by a linear gradient of 5~80% buffer B (water/acrylonitrile/formic acid, 5:95:0.2) over 120 minutes. MS/MS spectra were processed and analyzed using ProteinLynx Global Server (PLGS) 2.1 software (Micromass, UK). Lysyl acetylation was identified by the additional mass of 42 Daltons on lysine residue.

Statistics.

All data were analyzed using Microsoft Excel 2007 software, and results are expressed as means and standard deviations. I used the unpaired, two-sided

Student t-test to compare reporter activities and morphometric data from micro-CT analyses. Statistical significances were considered when P values were less than 0.05.

RESULTS

ARD1 is expressed in early bone formation stage.

To examine the role of ARD1 in bone formation, the expression of ARD1 was analyzed in preexisting and newly formed bones of rat calvarias which have a regional bone defect. The expression level of ARD1 was higher in osteoblasts around new bone surfaces compared to old bones (Fig. 1A). To understand the correlation of ARD1 and new bone formation, ARD1 expression was measured using bone building cells which named as the osteoblast such as primary mouse osteoblast cells (POB cells) and mouse mesenchymal precursor cells (C2C12 cells). In the primary mouse osteoblasts and C2C12 cells undergoing BMP-2-induced differentiation, the protein level of ARD1 was upregulated in parallel with Runx2 induction (Fig. 1B and Fig. 2A). Even in the absence of BMP-2, the protein levels of both Runx2 and ARD1 increased together during the late stage of the culture process (Fig. 1B). In mouse embryonic stage, both Runx2 and ARD1 were strongly expressed in vertebral bones on embryonic day 13 and declined gradually afterward (Fig. 3).

ARD1 negatively regulates osteoblast differentiation.

To examine the role of ARD1 in osteoblast differentiation, I measured alkaline phosphatase (ALP), OCN, BSP, and matrix mineralization which are well-

known markers of osteoblast differentiation. The depletion of ARD1 showed that acceleration of matrix mineralization using ALP staining and alizalin red S staining (Fig. 4-1A, B). The enzymatic activities and mRNA levels of ALP were also increased in ARD1 inhibition (Fig. 4-2C, D). The mRNA levels of OCN and BSP, known as makers of osteoblast differentiation and Runx2-related genes, were induced by ARD1-silencing (Fig. 4E). Accordingly, ARD1 was an inhibitory player in osteoblast differentiation induced by BMP-2 (Fig. 4). This action of ARD1 was also shown in MC3T3-E1 pre-osteoblast cells treated with BMP-2. In MC3T3-E1 cells, ARD1 inhibition showed augmentation of calcium accumulation, induction of ALP activities, and induction of BSP and OCN mRNA levels (Fig. 5). Therefore, ARD1 has negative role in osteoblast differentiation.

ARD1 selectively inhibits BMP-2-dependent osteoblast differentiation.

Besides BMP signaling pathways, the Wnt/β-catenin signaling pathway has been reported to play a role in osteoblast differentiation and maturation (Monroe et al., 2012). Furthermore, ARD1 has been reported to acetylate and activate β-catenin in lung cancer cell lines (Lim et al., 2006). However, the data presented in this study showed that ARD1 did not regulate Wnt3a-stimulated osteoblast differentiation. There seemed to be no change of mineralization between control group and ARD1 inhibition group during Wnt3a treatment (Fig. 6A). The mRNA levels of ALP and OCN were found to be induced in similar pattern at control and ARD1-silencing group (Fig. 6B,

C). Besides, the role of ARD1 in chondrocyte differentiation was examined since BMP signaling and the subsequent activation of Runx2 was already known to promote chondrogenesis (Nishimura et al., 2012). The results indicated that ARD1 was not upregulated in conjunction with Runx2 induction in chondrocytes (Fig. 7A). The depletion of ARD1 did not change expression of collagen, which is known for marker of chondrogenesis, by analyzing alcian blue staining (Fig. 7B). Also, the mRNA levels of Sox9 and Runx2, which are participated in chondrogenesis, appeared not to change during chondrocyte differentiation (Fig. 7C, D). These results suggest that ARD1 is not involved in chondrocyte differentiation. ARD1 may be restrictively involved in BMP-2-induced osteoblast differentiation.

Runx2 stabilizes ARD1 during osteoblast differentiation.

As Runx2 and ARD1 are co-induced during osteoblast differentiation, I checked the possibility that they regulate each other. When Runx2 was knocked down during osteoblast differentiation, the protein expression of ARD1 was repressed (Fig. 8A). Runx2 was required for the BMP-2 induction of ARD1, whereas ARD1 did not affect Runx2 expression (Fig. 8B). This role of Runx2 in ARD1 expression was confirmed using primary osteoblasts from heterozygous Runx2 knock-out mice (Fig. 8C). The expression of ARD1 was repressed in Runx2 knock-out mice-driven primary osteoblast cells during osteoblast differentiation. Then the mechanism underlying the Runx2 regulation of ARD1 was investigated. Runx2 was not involved in the

expression of ARD1 mRNA (Fig. 8A, D). To examine whether Runx2 regulates ARD1 protein, it was ectopically expressed GFP-ARD1 and found that Runx2 upregulated ARD1 at the post-translational level during osteoblast differentiation (Fig. 8E). The stability of ARD1 protein was checked by monitoring its level after blocking de novo protein synthesis (Fig. 9B, D, E). When Runx2 expressed, ARD1 stability was increased (Fig. 9A). However, it appeared that depletion of Runx2 destabilized ARD1 (Fig. 9C). ARD1 protein was stabilized Runx2-dependently. Given a previous report demonstrating that IkBα kinase β (IKKβ) phosphorylates ARD1 at Ser209 and by doing so destructs it through the proteasomes (Kuo et al., 2009), I examined whether IKKβ is involved in the Runx2 regulation of ARD1. IKKβ knock-down reversed the ARD1 destabilization by Runx2 knock-down (Fig. 9C). Furthermore, IKKβ was negatively regulated by Runx2 during osteoblast differentiation (Fig. 2A, 10A, 10B). Reversely, the expression of Runx2, it gradually decreased expression of IKKβ during BMP-2-dependent differentiation. As expected, IKKβ induced the serine-phosphorylation of ARD1, which determine ubiquitin-dependent degradation of ARD1. When Runx2 was silenced, the phosphorylation of serine at ARD1 was increased, which reduced the protein levels of ARD1 (Fig. 10C). Similarly with the depletion of IKKβ, Runx2 overexpression caused reduction phosphorylated serine residue in ARD1 and accumulation of ARD1 (Fig. 10D). Interestingly, both Runx2 and IKKβ silencing extremely repressed of serine-

phosphorylation of ARD1. This result supported that IKKβ leads phosphorylation of serine residue of ARD1, which is inhibited by Runx2. The results suggest that Runx2 stabilizes ARD1 during osteoblast differentiation through its inhibition of IKKβ-mediated phosphorylation and degradation of ARD1.

ARD1 inhibits Runx2 functionally.

ARD1′s control of Runx2 function was examined by using 6XOSE-luciferase and OG2-luciferase reporters having the Runx2 response element. The activities of both 6XOSE-luciferase and OG2-luciferase were repressed ARD1-dependently (Fig. 11A). The depletion of ARD1 showed that the transcription activities of Runx2 were further increased. This action of ARD1 was also shown in ARD1-deficient stable cell lines (Fig. 11B). Accordingly, the Runx2-driven transcription is negatively regulated by ARD1. Furthermore, BMP-2 stimulated Runx2 binding to the OCN promoter, which was augmented in the absence of ARD1 (Fig. 11C). These results suggest the inhibitory role of ARD1 in Runx2-driven gene expression.

ARD1 inhibits bone regeneration in adult rats.

Because injured bone is regenerated through osteoblastogenesis, the role of ARD1 in bone regeneration was examined in a rat calvarial critical-size defect model. Calvarial defects were covered with collagen matrices containing

shRNA viruses, and six weeks later calvarias were examined by micro-CT to evaluate the extent of bone formation (presented in green). New bone growth occurred inward from margins of calvarial holes covered with BMP-2 matrices, which was substantially augmented by ARD1 shRNA viruses (Fig. 12A). It was performed the 3-D morphometric measurement to analyze the extent to which the calvarial bones healed. Bone regeneration was significantly enhanced by BMP-2 and ARD1 shRNA in combination (Fig. 12B). H&E and von Kossa staining results provided further support the bone regeneration which is facilitated by ARD1 inhibition (Fig. 12C).

ARD1 negatively regulates bone development in mice.

To understand the role of ARD1 in bone development, the maturation of calvarias during the neonatal stage was examined in wild type and ARD1 transgenic mice. His/Myc-tagged ARD1 expression vector was used to generate two lines of transgenic mice (Lee et al., 2010). Endogenous and transgenic ARD1s were ubiquitously expressed in the skeletons containing bones and cartilages. Especially, calvaria, tibia and spine of ARD1 transgenic mice expressed both human and mouse ARD1 by analyzing of anti-ARD1 and anti-His antibodies. Also, major organs of transgenic mice also expressed endogenous and transgenic ARD1s (Fig. 13 and 14). There were no substantial differences in the gross skeletal structures between transgenic mice and wild type littermates on day 3 after birth (Fig. 15, left). Both wild type and transgenic mice showed similar stature, femur and clavicles length.

According to micro-CT analyses, however, calvarial fontanels of ARD1 transgenic mice #10 and #15 were less closed and the bones were less dense, compared with those of their littermates (Fig. 16A). Morphometric analyses show that calvarial area and density were significantly reduced in ARD1 transgenic mice (Fig. 16B, C). The negative role of ARD1 in bone development was rechecked using ARD1 knock-out mice. Homozygous ARD1 knock-out was verified by checking ARD1 levels in the skeletons and other organs (Fig. 17). The absence level of ARD1 in each organ of ARD1-depleted mice was confirmed by western blotting and immunohistochemistry. On day 3 after birth, the skeletal structure appears apparently similar between wild type and ARD1 knock-out mice, but many bones of knock-out mice were more densely stained by Alizarin Red than those of wild type mice (Fig. 15, right). In microCT images, calvarial bones were more developed in male and female ARD1 knock-out mice compared to wild type mice (Fig. 18). To recheck the inhibitory action of ARD1 on osteoblast differentiation at the cellular level, primary osteoblasts were isolated from the calvarias of wild type, ARD1 transgenic and ARD1 knock-out mice. As I assumed, BMP2-induced osteoblast differentiation is negatively regulated by ARD1 (Fig. 19). ARD1 transgenic expression decreased ALP activity, matrix mineralization, and mRNA levels of OCN and BSP. Reversely, ARD1 knock-out increased marker for osteoblast differentiation. Taken together, these results strongly indicate the negative role of ARD1 in bone development.

ARD1 binds and acetylates Runx2.

Next, it was addressed the molecular action of ARD1 in the Runx2 signaling pathway. ARD1 was combined with Runx2 in primary osteoblast cells and C2C12 cells (Fig. 20A). The binding was increased during BMP-2-dependent osteoblast differentiation. Accordingly, ARD1 physically interacts with Runx2 in differentiating osteoblasts. This interaction also occurred between ARD1 and Myc-Runx2 expressed in HEK293T cells (Fig. 20B). Since ARD1 can acetylate the ε-amino group of lysines, it was examined whether ARD1 lysyl-acetylates Runx2. Runx2 under BMP-2 stimulation was basally lysyl-acetylated in osteoblasts and this acetylation occured ARD1-dependently (Fig. 21A). This acetylation was silenced in ARD1 knock-out mice-driven primary osteoblast cells (Fig. 21B). ARD1-dependent acetylation also occurred between ARD1 and Myc-Runx2 expressed in HEK293T cells and disappeared in the absence of ARD1 (Fig. 21C). To indentify the Runx2 domain targeted by ARD1, one of four Flag/SBP-tagged Runx2 fragments were established, which were NT, N-terminus; RD, RUNT domain; PD, PST domain; CT, C-terminus. The fragments were co-expressed with ARD1 in HEK293T cells, and then pulled down using Streptoavidin-affinity resins. Of these fragments, RD peptide not only co-precipitated with ARD1 but was also acetylated by ARD1 (Fig. 22A), suggesting that ARD1 binds and acetylates the RUNT domain of Runx2. Although Runx2 was localized to the nucleus in osteoblasts, ARD1 was present mainly in the cytoplasm, where it interacts with Runx2 (Fig. 23). BMP-2 strongly activated the interaction with Runx2 and ARD1 in

cytosol. These results suggest that Runx2 is targeted by ARD1 in the cytoplasm before it enters into the nucleus or while it shuttles between the nucleus and the cytoplasm (Pockwinse et al., 2006). To identify the responsible entity for the reversal of the ARD1-mediated acetylation of the RUNT domain, I searched for the deacetylase among HDAC members. Of the six HDACs tested, HDAC6 blocked the ARD1-dependent RUNT acetylation (Fig. 22B). Given that HDAC6 was expressed at a constant level during osteoblast differentiation (Fig. 2A), the regulation of Runx2 acetylation is considered to be determined more by ARD1 than by HDAC6.

ARD1 interacts and acetylates Runx2 Lys225 in its RUNT domain.

To seek for acetylated residues of the RUNT domain, the RUNT peptide was purified in two steps and subjected to LC/MASS spectrometry (Fig. 24A). K183 and K225 of Runx2 are identified to be acetylated (Fig. 24B, C). A BLAST search (NCBI) revealed that both lysine residues are conserved in various species (Fig. 25A). To identify the lysine residue targeted by ARD1, I examined whether RUNT peptide and its mutants, which were namely K183R and K225R, were acetylated ARD1-dependently. The K225 residue in Runx2 is a specific site where is acetylated by ARD1, its direct acetylation was confirmed by Western blotting (Fig. 25B). The RUNT and K225R peptides were purified in two steps and performed LC/MASS spectrometry. Properly, the K225 mutant had no detection of acetylation (Fig. 26). To confirm lysine 225 residue at Runx2 is target site, *in vitro* acetylation assay was measured.

While GST-RD peptide was acetylated by His-ARD1 with Acetyl-CoA, GST-RD-K225R peptide had no influence (Fig. 27). Consequently, ARD1 binds and acetylates the lysine 225 residue of Runx2.

ARD1 interrupts the interaction between Runx2 and CBFβ by acetylating Lys225 at Runx2.

In addition, it was functionally checked the effect of the lysyl-acetylation on Runx2-driven transcription, and found that the ARD1-dependent K225 acetylation in Runx2 demoted the Runx2-driven transcription (Fig. 28A). In addition, the K225 acetylation disturbed the Runx2 binding to the OCN gene (Fig. 28B). As for the mechanism underlying the Runx2 inactivation by ARD1, I thought the possibility that ARD1 dissociates CBFβ from Runx2 because the transcription co-activator CBFβ interacts with the RUNT domain as ARD1 does. Runx2 directly interacted with CBFβ in HEK293T cells. When ARD1 was overexpressed, this interaction was interrupted (Fig. 29A). Through reversed immunoprecifitation, the interaction with Runx2 and CBFβ were gradually disappeared ARD1 dose-dependently (Fig. 29B). Also, this obstruction was not occurred in Runx2 K225R mutants (Fig. 29C). These results suggest that ARD1 interferes with CBFβ binding to Runx2 by acetylating Runx2 at K225.

ARD1 is a solo player for modulation of osteoblast differentiation.

In present studies, ARD1 is known as the catalytic subunit of NatA that acetylates the α-amino group (reference). NatA builds a complex, which is contained acetyltransferase such as ARD1 and NAA15. To understand whether ARD1 is required to support other enzymes, I analyzed Runx2-driven transcription with NAA15. While NAA15 knock-down greatly, there were not to change in ALP staining (Fig. 30A, B). ARD1 overexpression decreased Runx2 transcriptional activities. However, depletion of NAA15 had no further effect in activities of both 6XOSE-luciferase and OG2-luciferase (Fig. 30C, D). Therefore, NAA15 is not required for action of ARD1 and ARD1 has its enzymatic activity in osteoblast differentiation as a monomer.

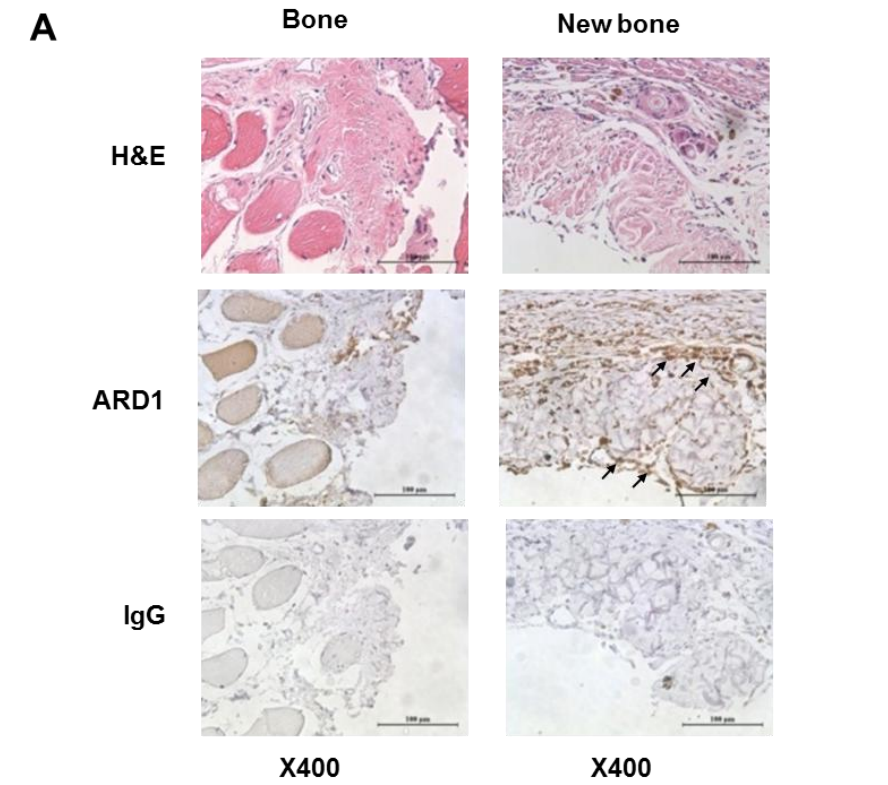
A
Bone
New bone
H&E
ARD1
IgG
X400
X400
B
Days 0 4 7 14 21
+ BMP-2
Runx2
1.00 2.45 1.67 0.42 1.28
ARD1
1.00 2.52 1.75 0.99 0.96
Tubulin
- BMP-2
Runx2
1.00 0.70 0.98 1.25 1.61
ARD1
1.00 0.91 1.10 1.26 1.31
Tubulin
Primary OB
+ BMP-2
Runx2
1.00 4.59 4.57 2.16 2.82
ARD1
1.00 4.87 3.51 2.56 1.68
Tubulin
C2C12

Figure 1. **ARD1 negatively regulates osteoblast differentiation.**

(A) A rat calvarial bone was punched out and covered with a collagen sponge containing 1 mg of BMP-2. After two months, the bone was removed, fixed, decalcified, paraffin-embedded, and cut into 5 μm sections. The sections including the margin of defect were stained with hematoxylin and eosin, or immunostained with anti-ARD1. Arrows indicate ARD1-positive osteoblasts. (B) Primary osteoblasts and C2C12 cells were incubated with PBS or BMP-2 (100 ng/ml) for the indicated times. Protein levels in lysates were analyzed by Western blotting using the indicated antibodies, and quantified using ImageJ. Runx2 and ARD1 values were divided by tubulin values and the ratios are expressed with respect to those at zero time.

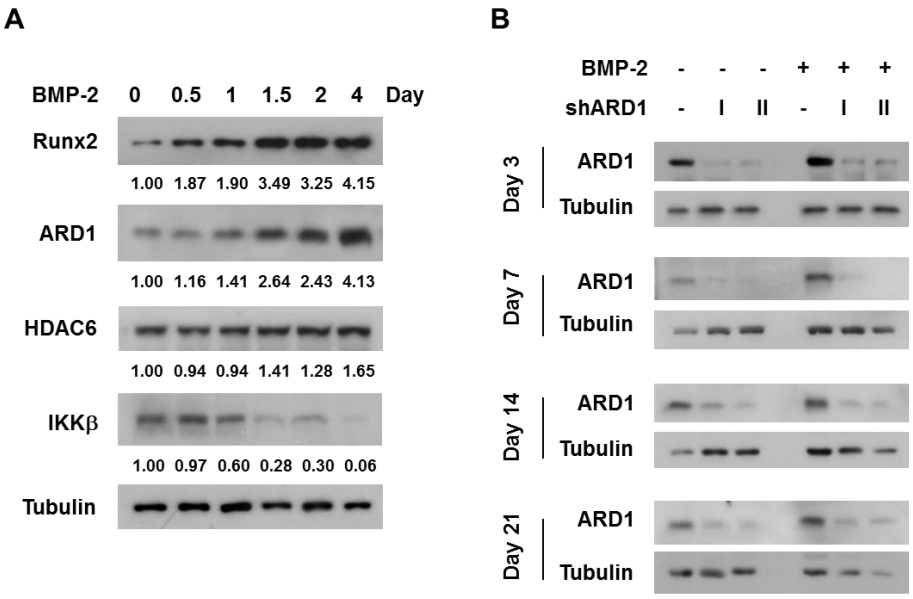
A
BMP-2 0 0.5 1 1.5 2 4 Day
Runx2
1.00 1.87 1.90 3.49 3.25 4.15
ARD1
1.00 1.16 1.41 2.64 2.43 4.13
HDAC6
1.00 0.94 0.94 1.41 1.28 1.65
IKKβ
1.00 0.97 0.60 0.28 0.30 0.06
Tubulin
B
BMP-2 - - - + + +
shARD1 - I II - I II
Day 3
ARD1
Tubulin
Day 7
ARD1
Tubulin
Day 14
ARD1
Tubulin
Day 21
ARD1
Tubulin

Figure 2. ARD1 is expressed during osteoblast differentiation.

(A) In primary osteoblasts treated with BMP-2 (100 ng/ml) for the indicated times, Runx2, ARD1, HDAC6, IKKβ and β-tubulin protein levels were analyzed by Western blotting. The blots were quantified (intensity x area) using ImageJ, and the results were divided by corresponding tubulin values. The protein levels were relatively compared with those at zero time. (B) C2C12 cells, which had been infected with ARD1-targeting shRNA viruses, were differentiated with BMP-2. On the indicated dates, ARD1 levels were analyzed in cell lysates by Western blotting.

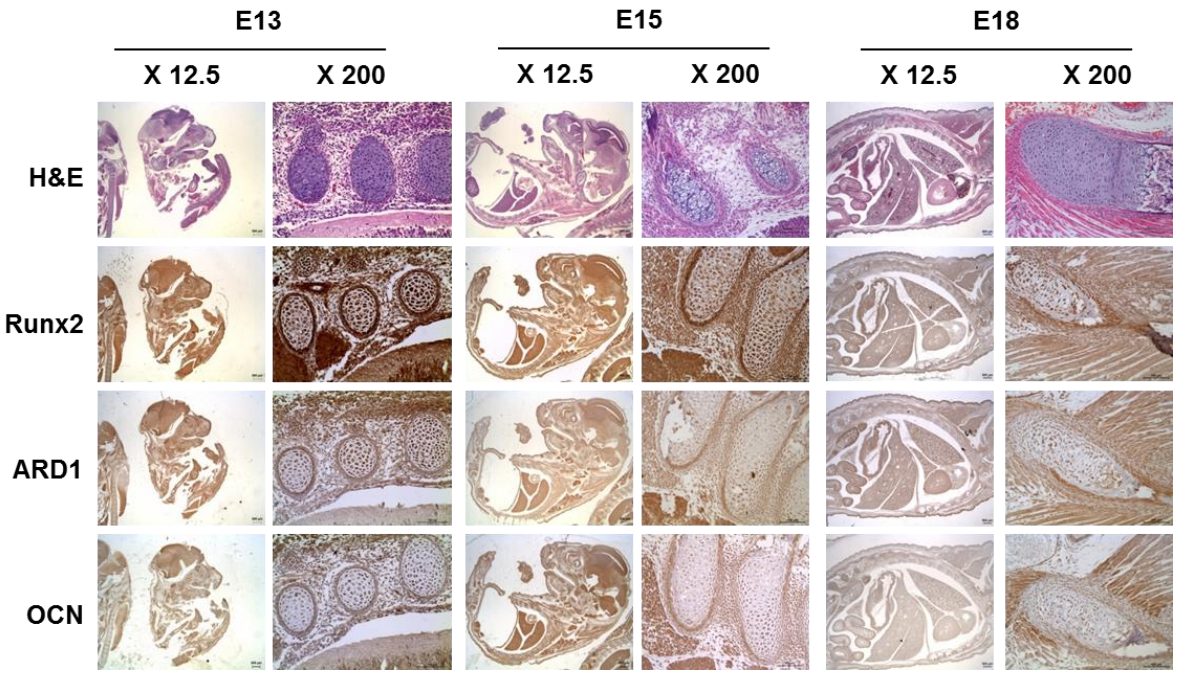
E13
E15
E18
X 12.5
X 200
X 12.5
X 200
X 12.5
X 200
H&E
Runx2
ARD1
OCN

Figure 3. Runx2 and ARD1 expressions in embryonic stage.

Paraffin sections of mice at E13, E15, and E18 were stained with H&E and subjected to immunohistochemical analyses using anti-Runx2, anti-ARD1, or anti-OCN antibody. Scale bar = 500 μm.

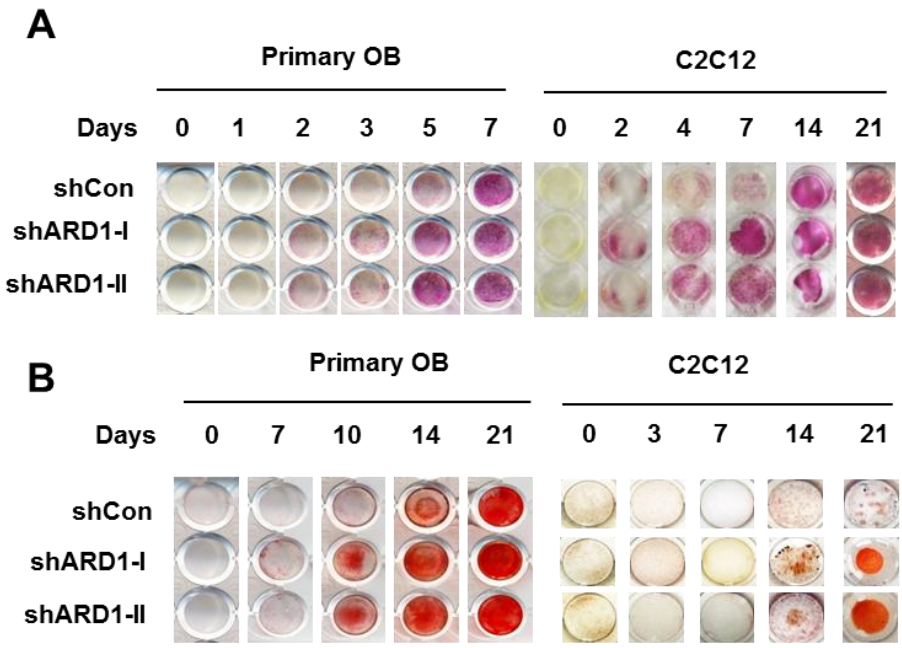
A
Primary OB
C2C12
Days
0
1
2
3
5
7
0
2
4
7
14
21
shCon
shARD1-I
shARD1-II
B
Primary OB
C2C12
Days
0
7
10
14
21
0
3
7
14
21
shCon
shARD1-I
shARD1-II

Figure 4-1. ARD1 inhibition increases osteoblast differentiation.

(A) Osteoblasts, which had been infected with non-targeting (shCon) or two different ARD1-targeting (shARD1) shRNA viruses, were differentiated with BMP-2. ALP was stained with naphthol AS-MX phosphate. (B) Mineralization in differentiating osteoblasts was stained with Alizarin Red S. The results are representative pictures of three independent experiments.

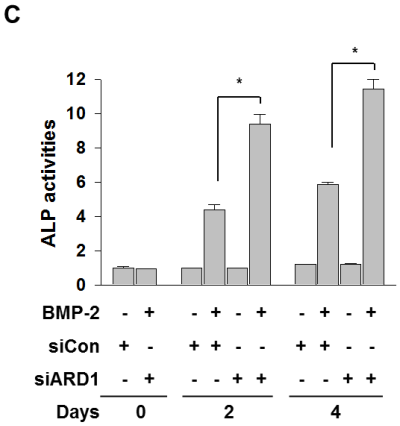
C
ALP activities
12
10
8
6
4
2
0
*
*
BMP-2 - + - + - + - + - +
siCon + - + + - - + + - -
siARD1 - + - - + + - - + +
Days 0 2 4

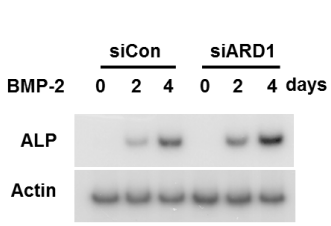
D
siCon
siARD1
BMP-2 0 2 4 0 2 4 days
ALP
Actin

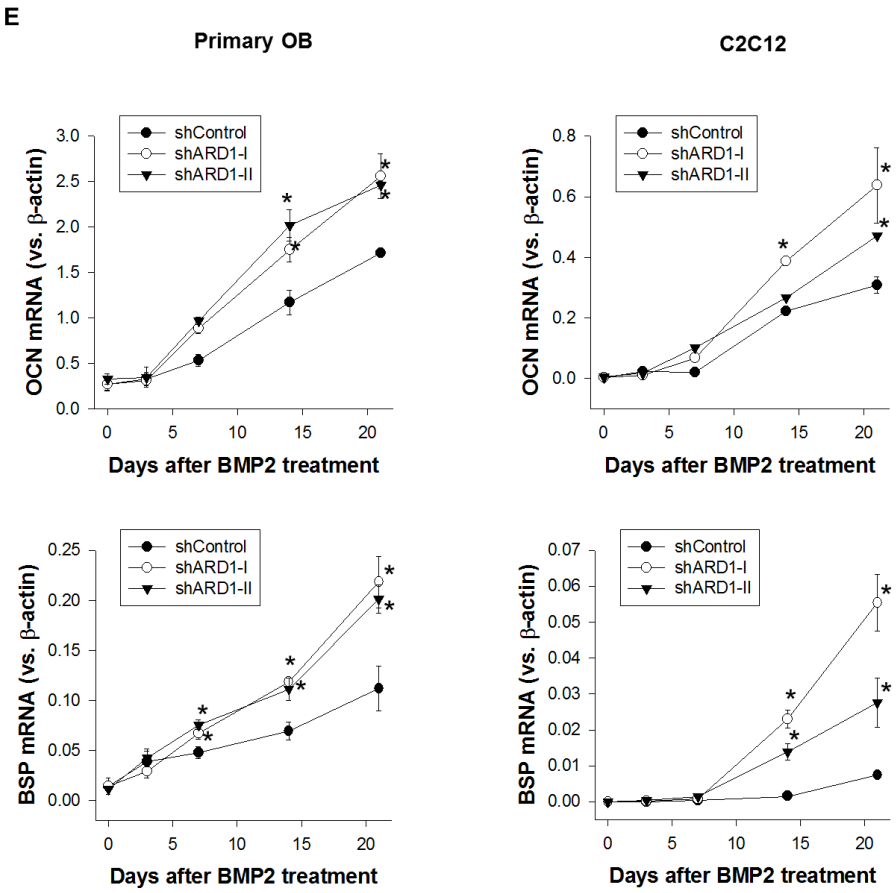
E
Primary OB
C2C12
shControl
shARD1-I
shARD1-II
OCN mRNA (vs. β-actin)
BSP mRNA (vs. β-actin)
Days after BMP2 treatment
*

Figure 4-2. ARD1 inhibition increases osteoblast differentiation.

(c) C2C12 cells, which had been transfected with the indicated siRNAs, were treated with PBS or BMP-2 for 4 days. ALP activities (means±SDs, n=4) were normalized versus total protein levels and are presented as relative values versus controls. * denotes $P<0.05$. (D) RNAs were extracted from transfected C2C12 cells and reverse-transcribed. ALP and actin cDNAs were amplified using PCR over 17 to 22 cycles with [α-^{32}P]dCTP, and the cDNAs obtained were electrophoresed on 4% polyacrylamide gels and autoradiographed. (E) OCN and BSP mRNA levels were quantified in differentiating osteoblasts by RT-qPCR. Results are expressed as the means±SDs (n=4), and * denotes $P<0.05$ versus the shCon group.

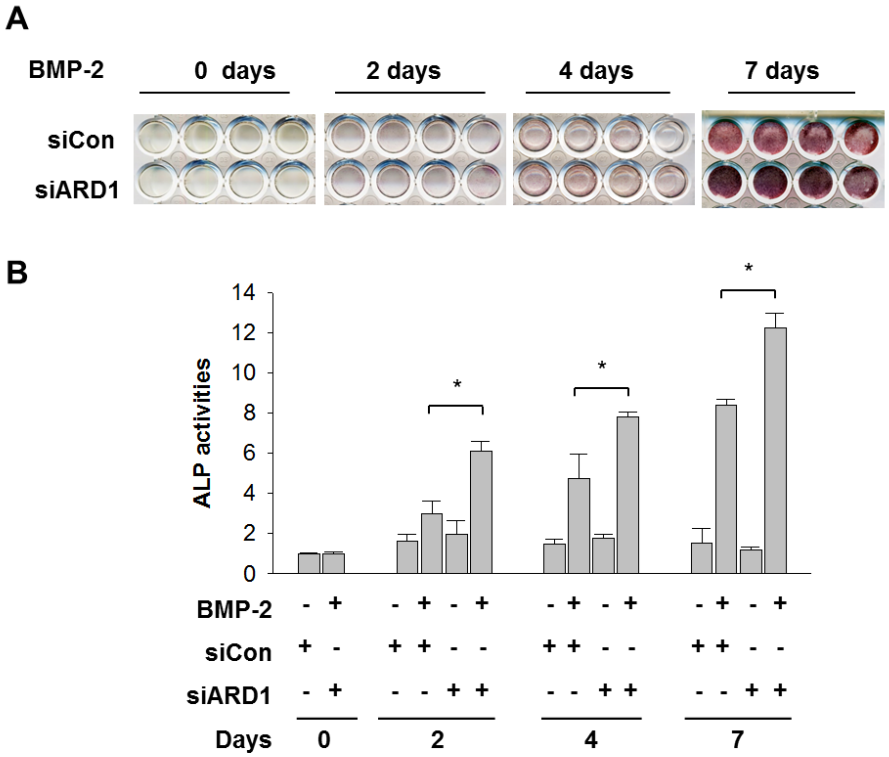
A
BMP-2
0 days
2 days
4 days
7 days
siCon
siARD1
B
ALP activities
14
12
10
8
6
4
2
0
*
*
*
BMP-2 - + - + - + - + - + - + - + - +
siCon + - + + - - + + - - + + - -
siARD1 - + - - + + - - + + - - + +
Days 0 2 4 7
C
OCN mRNA levels (folds)
16
14
12
10
8
6
4
2
0
siCon
siARD1
*
0 2 4
Days after BMP2 treatment
D
BSP mRNA levels (folds)
50
40
30
20
10
0
siCon
siARD1
*
0 2 4
Days after BMP2 treatment

Figure 5. ARD1 knock-down promotes osteoblast differentiation in MC3T3-E1 cells.

ARD1 or control siRNAs were transfected into MC3T3-E1 cells, and treated with BMP-2 (100 ng/ml) for the indicated times. Cells were stained with p-nitrophenyl phosphate (A) or lysed for enzymatic ALP assays (B). ALP activities (means±SDs, n=4) were normalized to protein amounts, and presented as relative values versus the mock and PBS control. RNAs were extracted from transfected MC3T3-E1 cells, and the osteocalcin (C) and BSP (D) mRNA levels were quantified by RT-qPCR. * denotes $P<0.05$.

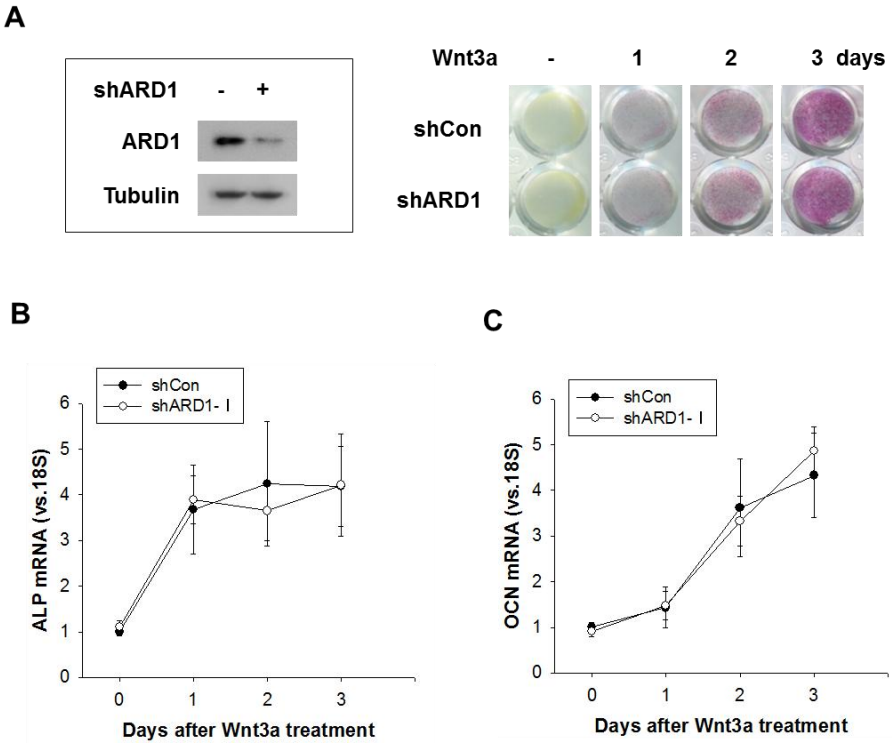
A
shARD1 - +
ARD1
Tubulin
Wnt3a - 1 2 3 days
shCon
shARD1
B
shCon
shARD1- I
ALP mRNA (vs.18S)
Days after Wnt3a treatment
C
shCon
shARD1- I
OCN mRNA (vs.18S)
Days after Wnt3a treatment

Figure 6. ARD1 is not involved in Wnt3a-induced osteoblast differentiation.

(A) C2C12 cells, which had been infected with *ARD1*-targeting shRNA viruses, were differentiated with Wnt3a (50 ng/ml) for the indicated days. ARD1 levels were analyzed Western blotting (left panel). Cells were stained with naphthol AS-MX phosphate at 37^{o}C for 1 hour (right panel). (B, C) The mRNA levels of ALP and OCN were quantified by RT-qPCR. Results are expressed as the means±SDs (n=4).

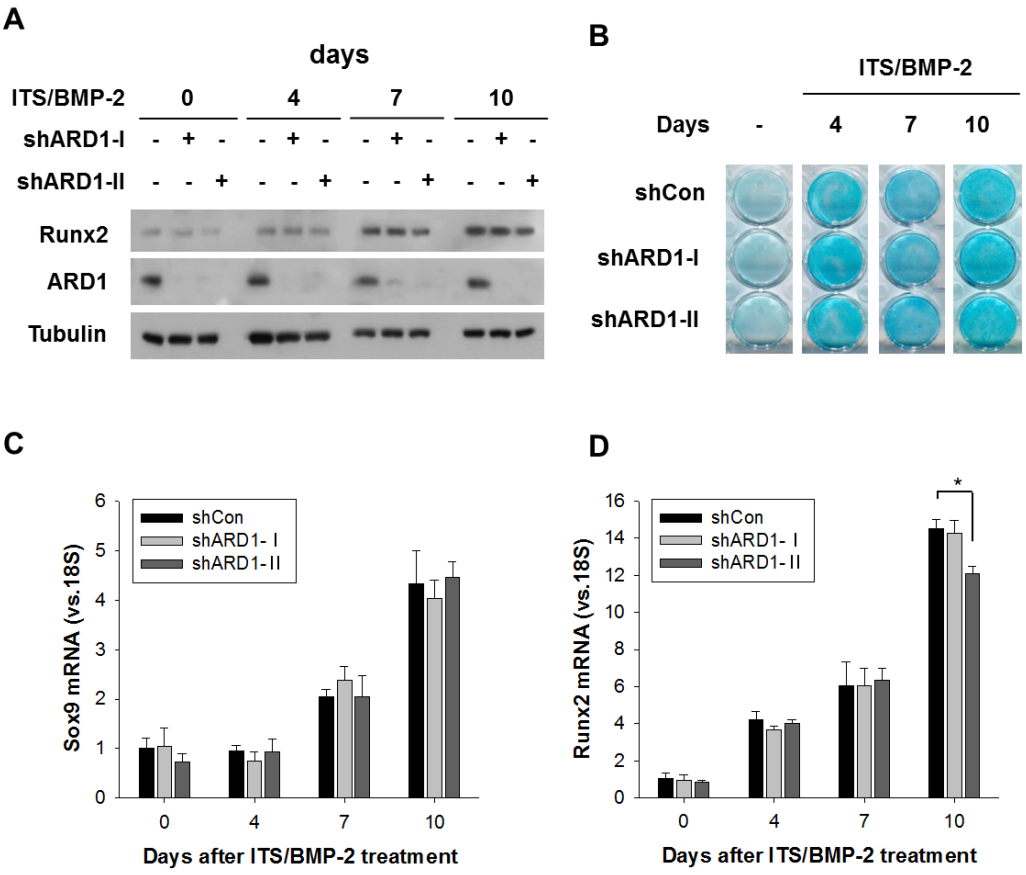
A
days
ITS/BMP-2
0
4
7
10
shARD1-I
shARD1-II
Runx2
ARD1
Tubulin
B
ITS/BMP-2
Days
-
4
7
10
shCon
shARD1-I
shARD1-II
C
shCon
shARD1- I
shARD1- II
Sox9 mRNA (vs.18S)
Days after ITS/BMP-2 treatment
D
shCon
shARD1- I
shARD1- II
Runx2 mRNA (vs.18S)
*
Days after ITS/BMP-2 treatment

Figure 7. ARD1 is not involved in chondrocyte differentiation.

Mouse Chondrogenic ATDC5 cells, which had been infected with *ARD1*-targeting shRNA viruses, were treated with ITS and BMP-2 (10 ng/ml) for the indicated days. (A) Runx2 and ARD1 levels were analyzed by Western blotting. (B) ATDC5 cells were stained with Alcian blue to evaluate chondrocyte differentiation. (C, D) Sox9 and Runx2 mRNA levels were quantified by RT-qPCR. Results are expressed as the means±SDs (n=4).

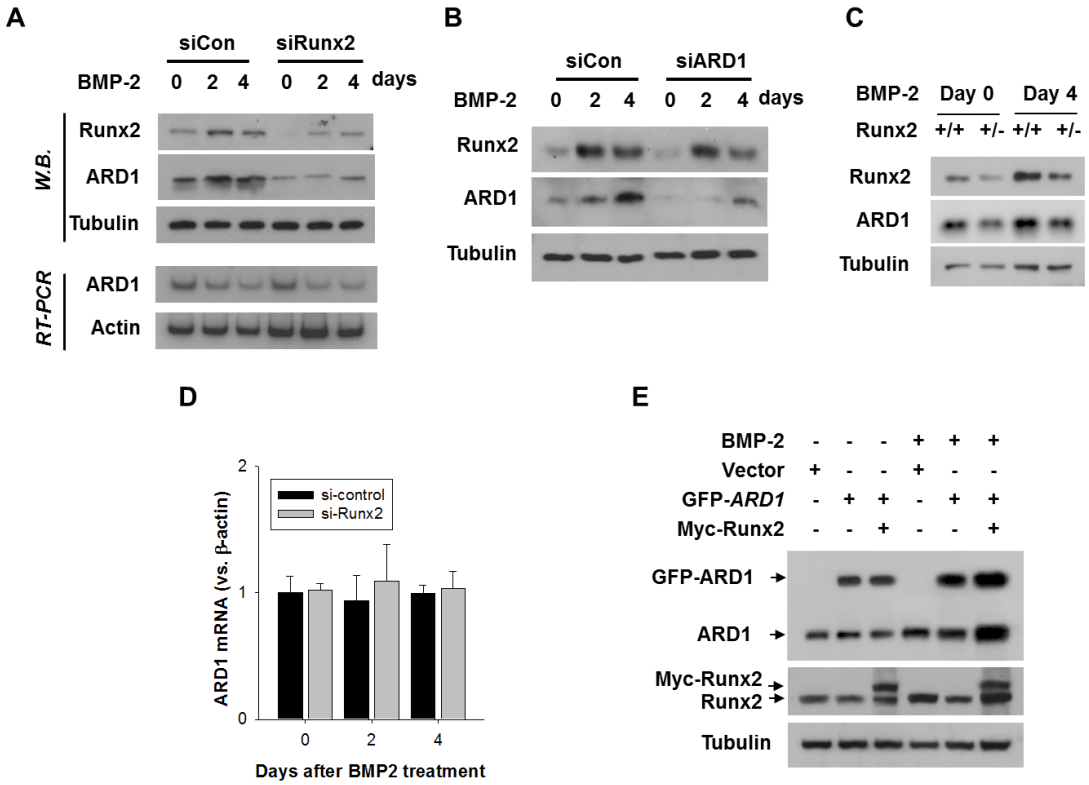
A
siCon
siRunx2
BMP-2 0 2 4 0 2 4 days
W.B.
Runx2
ARD1
Tubulin
RT-PCR
ARD1
Actin
B
siCon
siARD1
BMP-2 0 2 4 0 2 4 days
Runx2
ARD1
Tubulin
C
BMP-2 Day 0 Day 4
Runx2 +/+ +/- +/+ +/-
Runx2
ARD1
Tubulin
D
si-control
si-Runx2
ARD1 mRNA (vs. β-actin)
2
1
0
0 2 4
Days after BMP2 treatment
E
BMP-2 - - - + + +
Vector + - - + - -
GFP-ARD1 - + + - + +
Myc-Runx2 - - + - - +
GFP-ARD1
ARD1
Myc-Runx2
Runx2
Tubulin

Figure 8. ARD1 is stabilized Runx2-dependently during osteoblastogenesis.

(A) C2C12 cells, which had been transfected with 80 nM siRNA targeting Runx2, were treated with BMP-2 for 2 or 4 days. Runx2 and ARD1 expressions were analyzed by Western blotting or semiquatitative RT-PCR. (B) Primary osteoblasts were co-transfected with the plasmids of GFP-ARD1 (2 μg) and Myc-Runx2 (1 μg) and treated with BMP-2 for 2 days. Protein expressions were analyzed by Western blotting. (C) C2C12 cells, which had been transfected with 80 nM siRNA targeting ARD1, were treated with BMP-2 for 2 or 4 days. Runx2 and ARD1 expressions were analyzed by Western blotting. (D) Primary osteoblasts were isolated from wild type and $Runx2^{+/-}$ mice, both of which were provided by Dr. Hyun-Mo Ryoo (Seoul National University School of Dentistry, Korea). Cells were incubated with BMP-2 for 4 days, and Runx2 and ARD1 levels were analyzed by Western blotting. The heterozygous Runx knock-out (E) ARD1 mRNA levels were quantified by RT-qPCR in BMP-2 treated C2C12 cells which had been transfected with the indicated siRNAs. Results are expressed as the means±SDs (n=4).

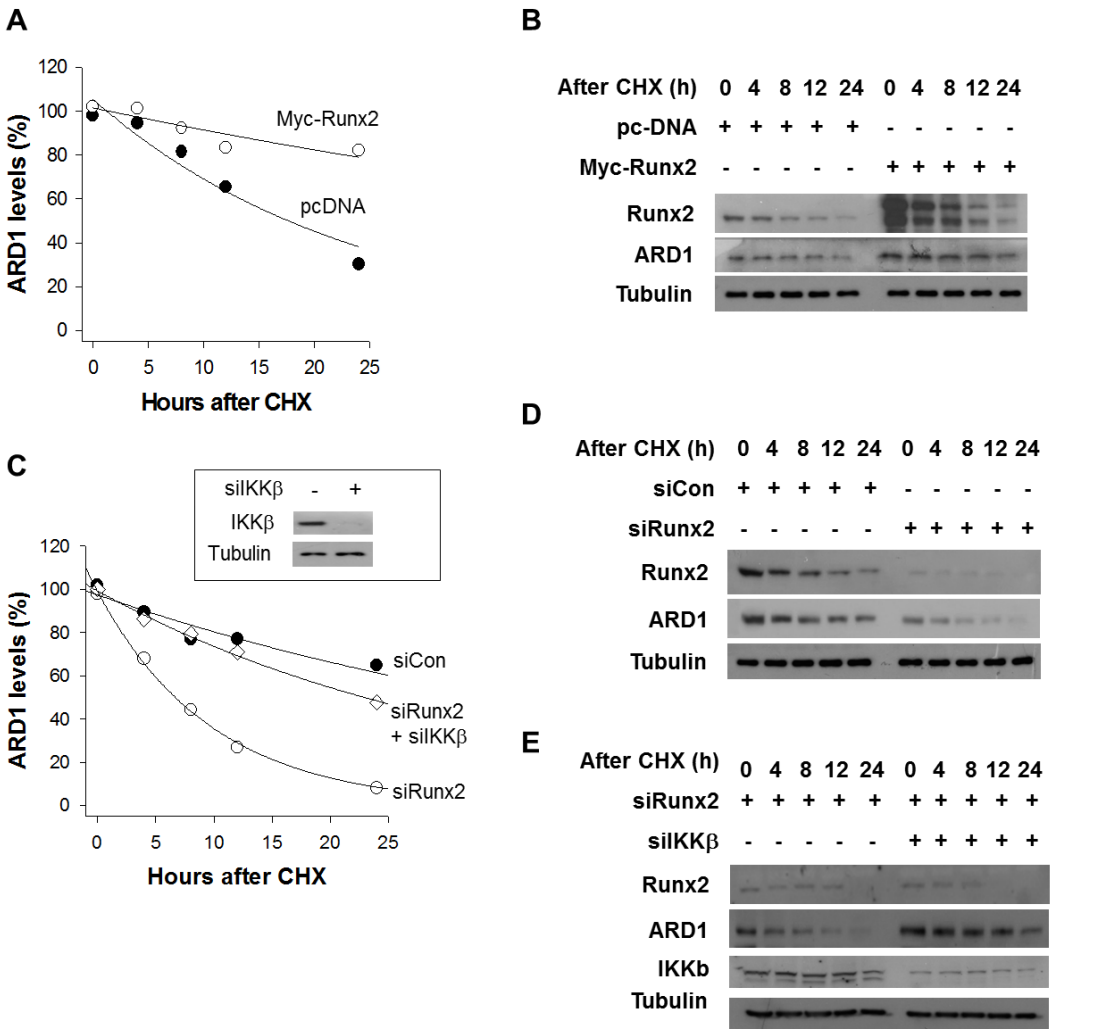
A
ARD1 levels (%)
Hours after CHX
Myc-Runx2
pcDNA
B
After CHX (h) 0 4 8 12 24 0 4 8 12 24
pc-DNA
Myc-Runx2
Runx2
ARD1
Tubulin
C
siIKKβ - +
IKKβ
Tubulin
siCon
siRunx2
+ siIKKβ
siRunx2
D
After CHX (h) 0 4 8 12 24 0 4 8 12 24
siCon
siRunx2
Runx2
ARD1
Tubulin
E
After CHX (h) 0 4 8 12 24 0 4 8 12 24
siRunx2
siIKKβ
Runx2
ARD1
IKKb
Tubulin

Figure 9. Runx2 blocks the ARD1 degradation induced by IKKβ.

(A, C) C2C12 cells, which had been transfected with Runx2 siRNA (80 nM) or plasmid (1 μg), were treated with 100 nM cycloheximide for the indicated times. ARD1 and tubulin levels were analyzed by Western blotting and quantified using ImageJ software. ARD1 values were divided by tubulin values and ARD1/tubulin ratios are expressed with respect to those at zero time.

(B) C2C12 cells, which had been transfected with Myc-Runx2 plasmid or pcDNA, were treated with 100 nM cycloheximide for the indicated times. (D) C2C12 cells were transfected with 80 nM Runx2 or control siRNAs, and treated with cycloheximide. (E) C2C12 cells were transfected with 80 nM Runx2 or/and IKKβ siRNAs, and treated with cycloheximide. Runx2 and ARD1 levels were analyzed by Western blotting.

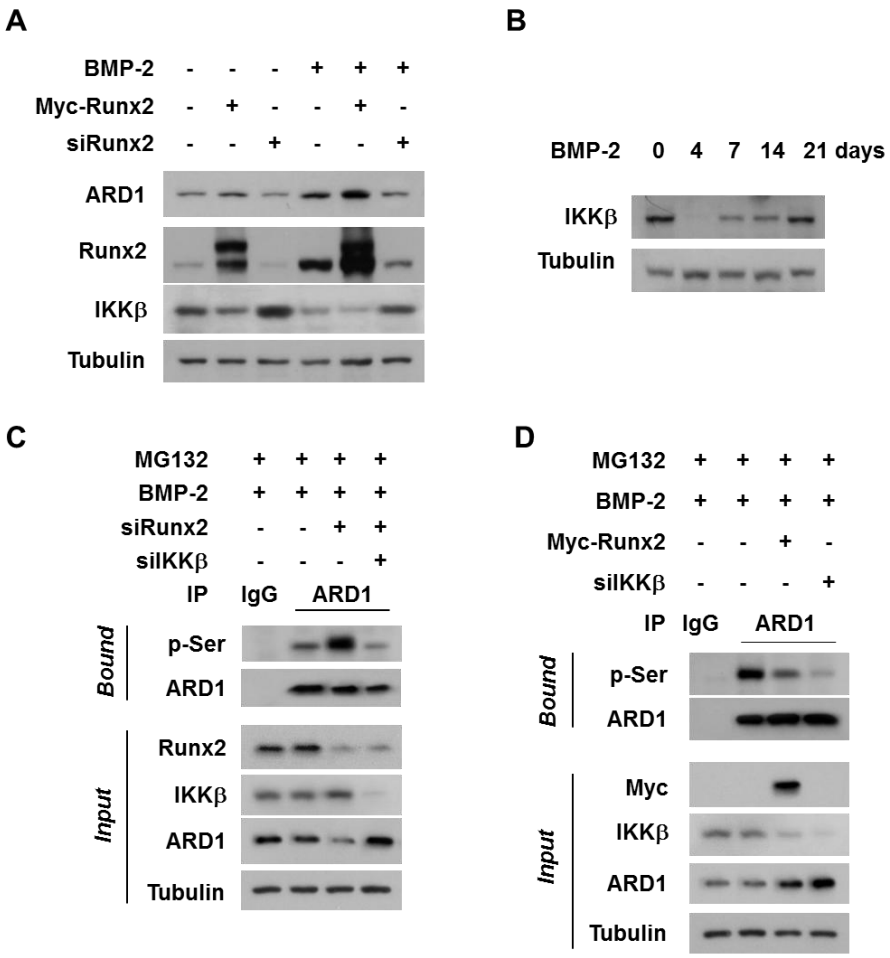
A
BMP-2 - - - + + +
Myc-Runx2 - + - - + -
siRunx2 - - + - - +
ARD1
Runx2
IKKβ
Tubulin
B
BMP-2 0 4 7 14 21 days
IKKβ
Tubulin
C
MG132 + + + +
BMP-2 + + + +
siRunx2 - - + +
siIKKβ - - - +
IP IgG ARD1
Bound
p-Ser
ARD1
Input
Runx2
IKKβ
ARD1
Tubulin
D
MG132 + + + +
BMP-2 + + + +
Myc-Runx2 - - + -
siIKKβ - - - +
IP IgG ARD1
Bound
p-Ser
ARD1
Input
Myc
IKKβ
ARD1
Tubulin

Figure 10. Runx2 inhibits IKKβ-dependent serine-phosphorylation of ARD1.

(A) Primary osteoblasts were transfected with the plasmids of Myc-Runx2 or Runx2 siRNA and treated with BMP-2 for 2 days. Expressed proteins were immunoblotted. (B) C2C12 cells, which were transfected with Runx2 and/or IKKβ siRNAs, were incubated with BMP-2 for 24 hours, and further treated with 20 μM MG132 for 8 hours. Cell lysates were immunoprecipitated with anti-ARD1, and the precipitates were immunoblotted with phosphoserine (p-Ser) antibody. The input levels of ARD1, Runx2 and IKKβ were verified by Western blotting. (C) C2C12 cells were treated with BMP-2 for the indicated times, and the IKKβ levels were analyzed by Western blotting. (D) C2C12 cells, which were transfected with Myc-Runx2 plasmid and/or IKKβ siRNA, were incubated with BMP-2 for 24 hours, and further treated with 20 μM MG132 for 8 hours. Cell lysates were immunoprecipitated with anti-ARD1, and the precipitates were immunoblotted with phosphoserine (p-Ser) antibody. The input levels of ARD1, Runx2 and IKKβ were verified by Western blotting.

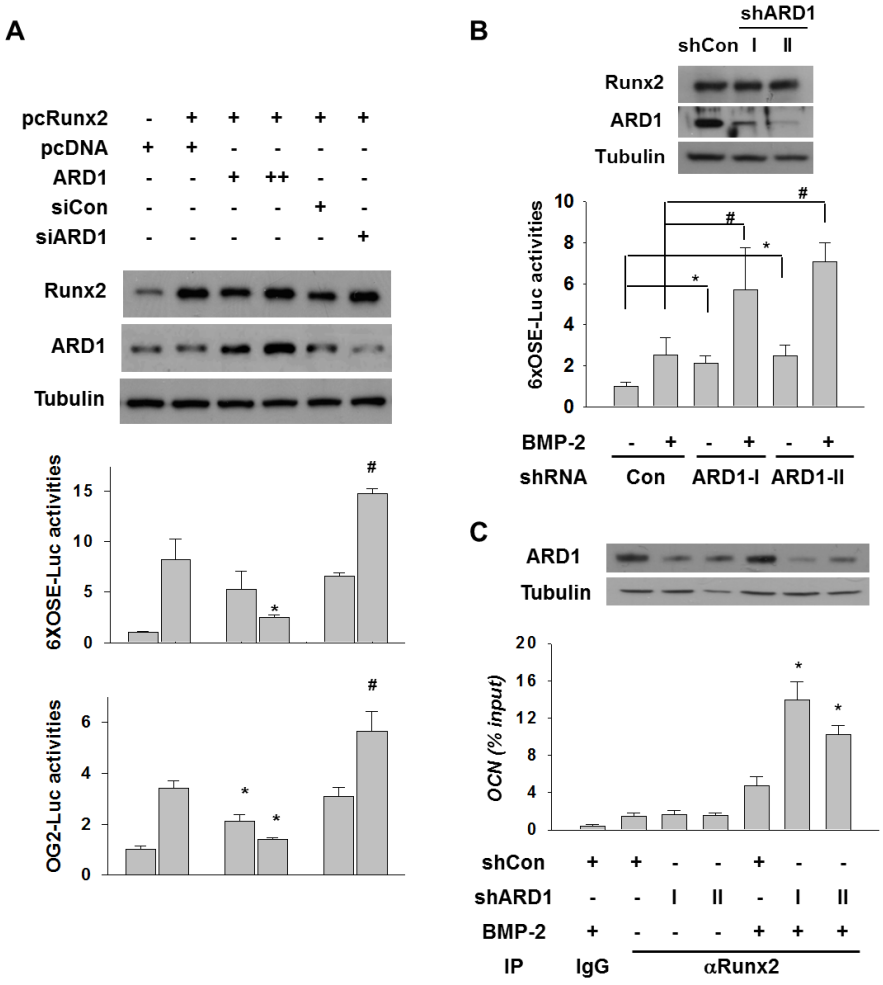
A
pcRunx2 - + + + + +
pcDNA + + - - - -
ARD1 - - + ++ - -
siCon - - - - + -
siARD1 - - - - - +
Runx2
ARD1
Tubulin
6XOSE-Luc activities
OG2-Luc activities
B
shARD1
shCon I II
Runx2
ARD1
Tubulin
6xOSE-Luc activities
BMP-2 - + - + - +
shRNA Con ARD1-I ARD1-II
C
ARD1
Tubulin
OCN (% input)
shCon + + - - + - -
shARD1 - - I II - I II
BMP-2 + - - - + + +
IP IgG αRunx2

Figure 11. ARD1 represses the transcriptional activity of Runx2.

(A) C2C12 cells were co-transfected with 1 μg of 6XOSE-luciferase plasmid or OG2-luciferase plasmid and β-gal plasmid and with 1 or 2 μg of Runx2 plasmid or 80 nM of Runx2 siRNA. After being allowed to stabilize for 24 hours, cells were lysed for Western blotting (top) or reporter assays (middle and bottom). Luciferase activities (means±SDs, n=4) were normalized versus β-gal activity, and are presented as relative values with respect to controls. * and # denote $P<0.05$ versus the pcDNA control and versus the siRNA control, respectively. (B) C2C12 cell lines infected with shARD1 were co-transfected with 6XOSE luciferase and β-gal plasmids, and treated with BMP-2 for 24 hours. Cells were lysed for Western blotting (top) and reporter (bottom) analyses. Luciferase/β-gal values (means±SDs, n=4) are presented as relative values versus BMP-2 (-) control shRNA. * and # denote $P<0.05$ versus BMP-2 (-) control shRNA and versus BMP-2 (+) control shRNA, respectively. (C) C2C12 cell lines infected with shARD1 or shControl virus were treated with BMP-2 for 48 hours and ARD1 levels were checked by Western blotting (top). Cells were then fixed with formalin and cross-linked chromatins were immunoprecipitated with non-immunized serum (IgG) or anti-Runx2. DNAs were eluted from precipitates and real-time PCR was performed to amplify the mouse osteocalcin (OCN) promoter region. * denotes $P<0.05$ versus the BMP-2 (+) shControl group.

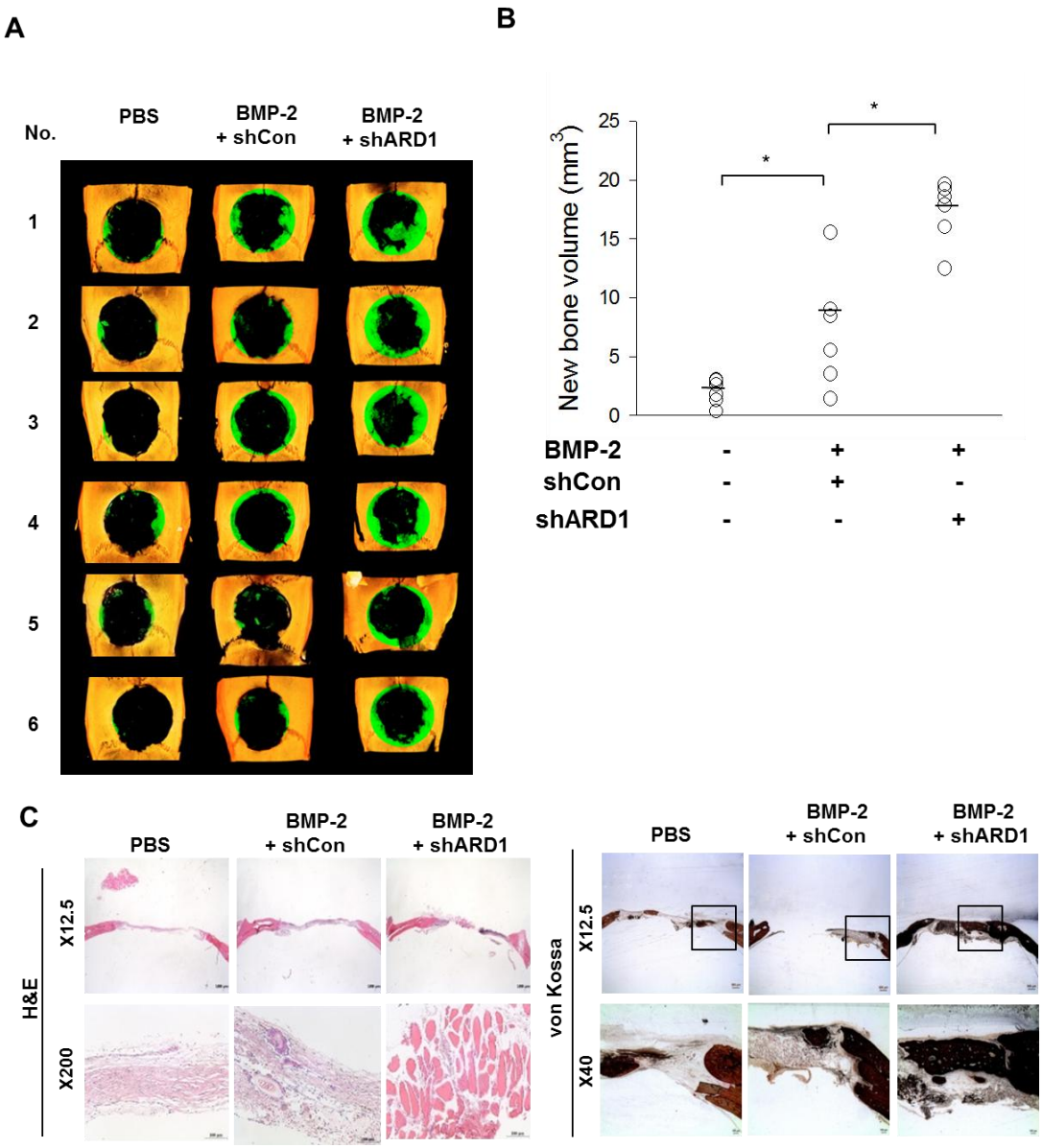
A
No.
PBS
BMP-2 + shCon
BMP-2 + shARD1
1
2
3
4
5
6
B
New bone volume (mm3)
25
20
15
10
5
0
*
*
BMP-2 - + +
shCon - + -
shARD1 - - +
C
H&E
X12.5
X200
PBS
BMP-2 + shCon
BMP-2 + shARD1
von Kossa
X12.5
X40
PBS
BMP-2 + shCon
BMP-2 + shARD1

Figure 12. ARD1 knock-down augments the healing of rat calvarial defects.

(A) Six rat calvarial bones per group were punched out and covered with collagen sponge containing BMP-2 (or PBS) and shARD1 virus (or shControl virus). Calvarias were removed on day 42 after surgery and subjected to micro-CT analysis to evaluate defect healing. Micro-CT images were reconstructed three dimensionally; bone ingrowth from defect margins are marked with green. (B) Volumes of ingrown bones were calculated using 3-D CT images. Short horizontal bars represent group mean values and * denotes $P<0.05$ between two groups. (C) Calvarial tissues were fixed, decalcified, embedded, and cut into 5 μm sections. The sections were stained with hematoxylin and eosin (H&E). Calvarial tissues were fixed, embedded, and cut into 50 μm sections. The sections were stained with von Kossa/Nuclear Fast Red. The images were captured under a microscope.

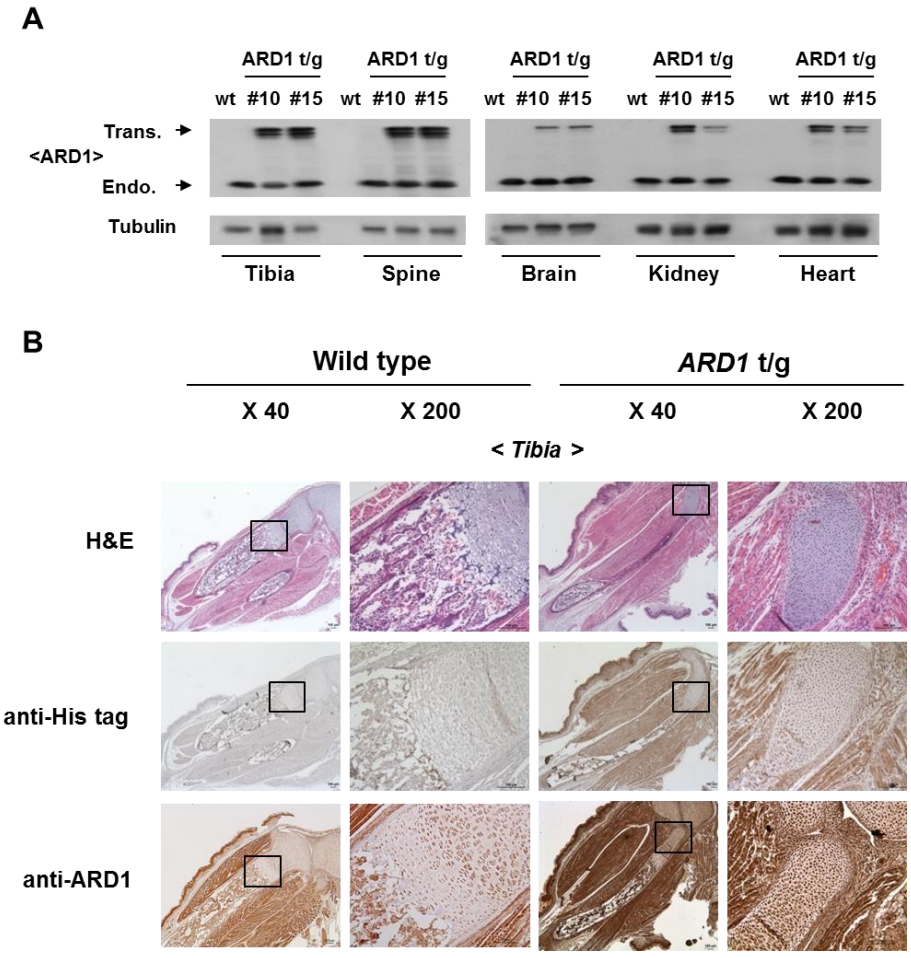
A
ARD1 t/g
ARD1 t/g
ARD1 t/g
ARD1 t/g
ARD1 t/g
wt #10 #15
wt #10 #15
wt #10 #15
wt #10 #15
wt #10 #15
Trans.
<ARD1>
Endo.
Tubulin
Tibia
Spine
Brain
Kidney
Heart
B
Wild type
ARD1 t/g
X 40
X 200
X 40
X 200
< Tibia >
H&E
anti-His tag
anti-ARD1

Figure 13-1. ARD1 expressions in ARD1 transgenic mouse.

(A) Expression of endogenous ARD1 (Endo.) and transgenic Myc/His-tagged ARD1 (Trans.) ARD1 in wild type and two ARD1 transgenic lines #10 and #15. Tissue homogenates were prepared from tibia, spine, brain, kidney, and heart, and analyzed by Western blotting with anti-ARD1 antibody. (B) Immunohistochemical analyses of ARD1 in wild type and ARD1 transgenic mice (#10). Paraffin tissue sections of mice at a postnatal 3 day were subjected to H&E staining (upper panel) and immunohistochemical analyses. Scale bar = 100 μm.

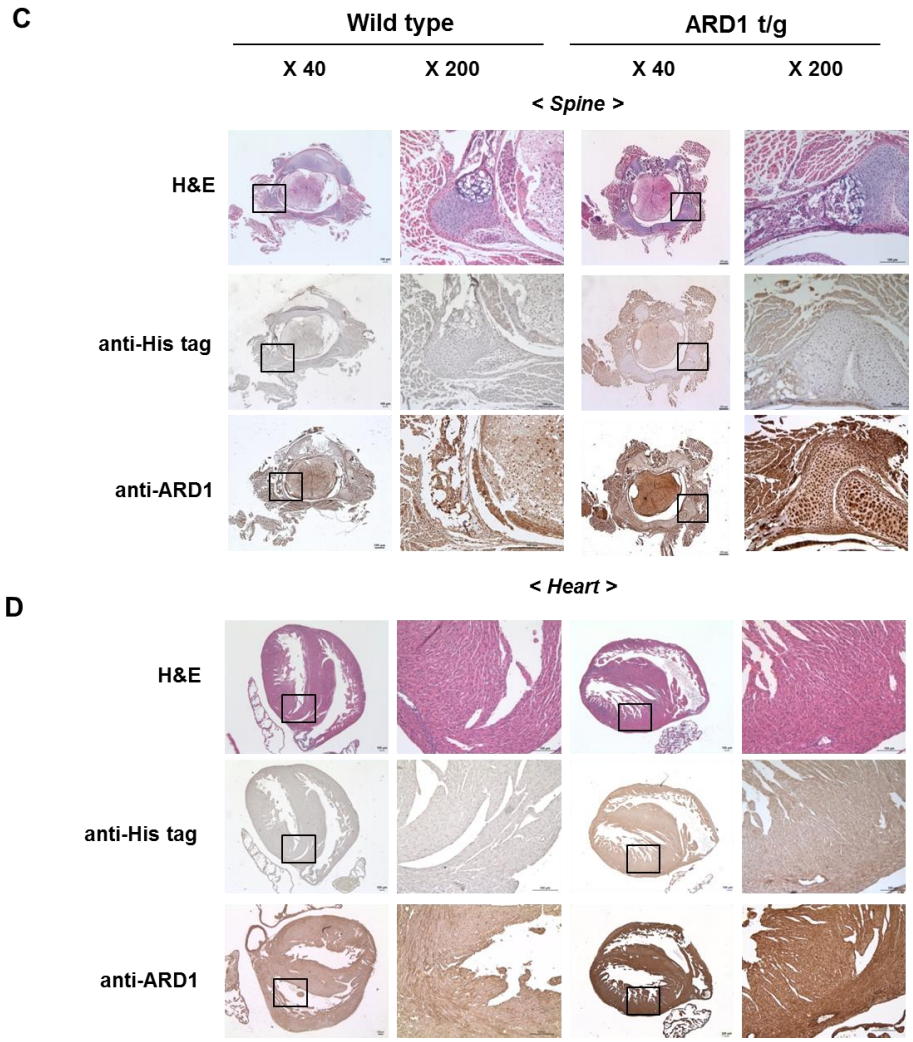
C
Wild type
ARD1 t/g
X 40
X 200
X 40
X 200
< Spine >
H&E
anti-His tag
anti-ARD1
< Heart >
D
H&E
anti-His tag
anti-ARD1

Figure 13-2. ARD1 expressions in ARD1 transgenic mouse.

(C, D) Immunohistochemical analyses of ARD1 in wild type and ARD1 transgenic mice (#10). Paraffin tissue sections of mice at a postnatal 3 day were subjected to H&E staining (upper panel) and immunohistochemical analyses. Scale bar = 100 μm.

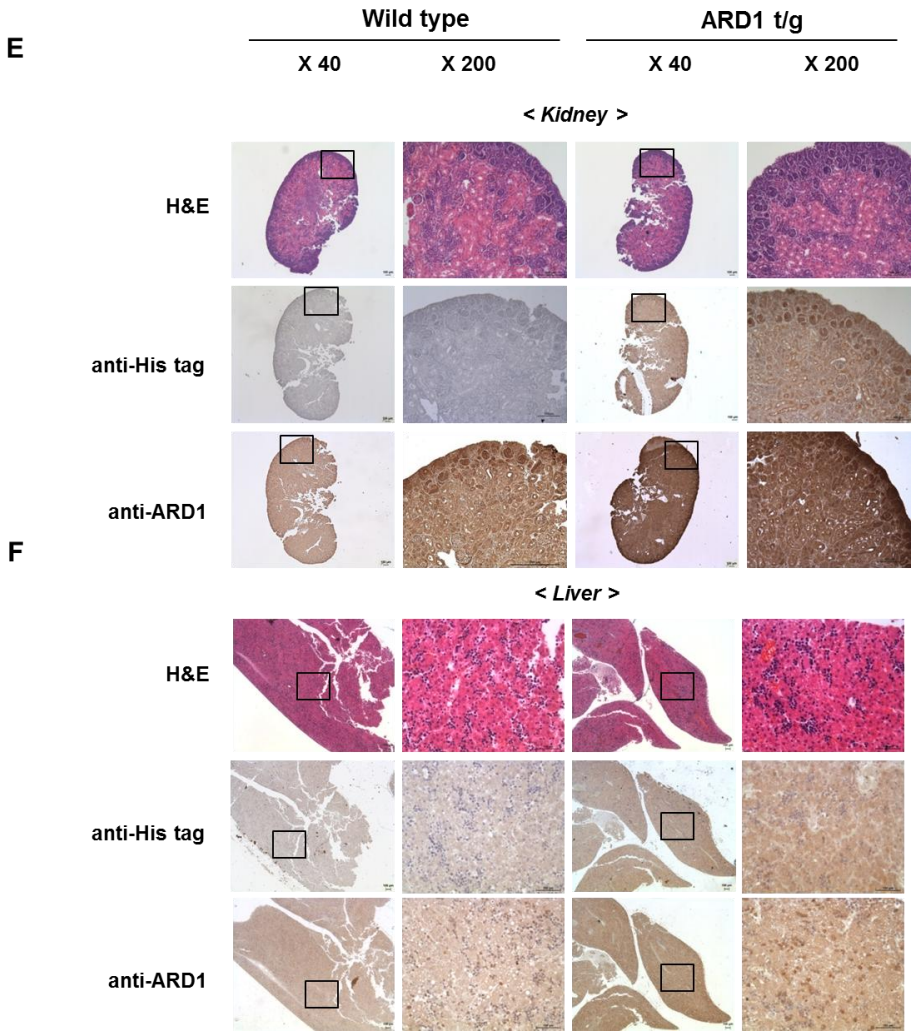
E
Wild type
ARD1 t/g
X 40
X 200
X 40
X 200
< Kidney >
H&E
anti-His tag
anti-ARD1
F
< Liver >
H&E
anti-His tag
anti-ARD1

Figure 13-3. ARD1 expressions in ARD1 transgenic mouse.

(E, F) Immunohistochemical analyses of ARD1 in wild type and ARD1 transgenic mice (#10). Paraffin tissue sections of mice at a postnatal 3 day were subjected to H&E staining (upper panel) and immunohistochemical analyses. Scale bar = 100 μm

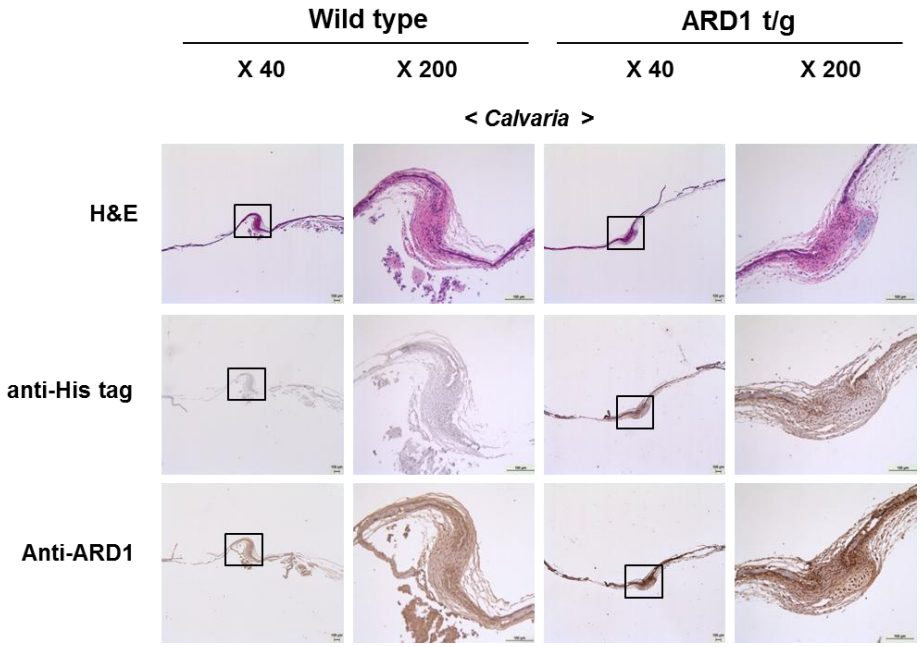
Wild type
ARD1 t/g
X 40
X 200
X 40
X 200
< Calvaria >
H&E
anti-His tag
Anti-ARD1

Figure 14. ARD1 expression in calvarias of ARD1 transgenic mice.

Paraffin sections of calvarias from wild type and Myc/His-tagged ARD1 t/g mice were stained with H&E (top panel), and subjected to immunohistochemical analyses with anti-His (middle panel) or anti-ARD1 antibody (bottom panel). Scale bar = 100 μm.

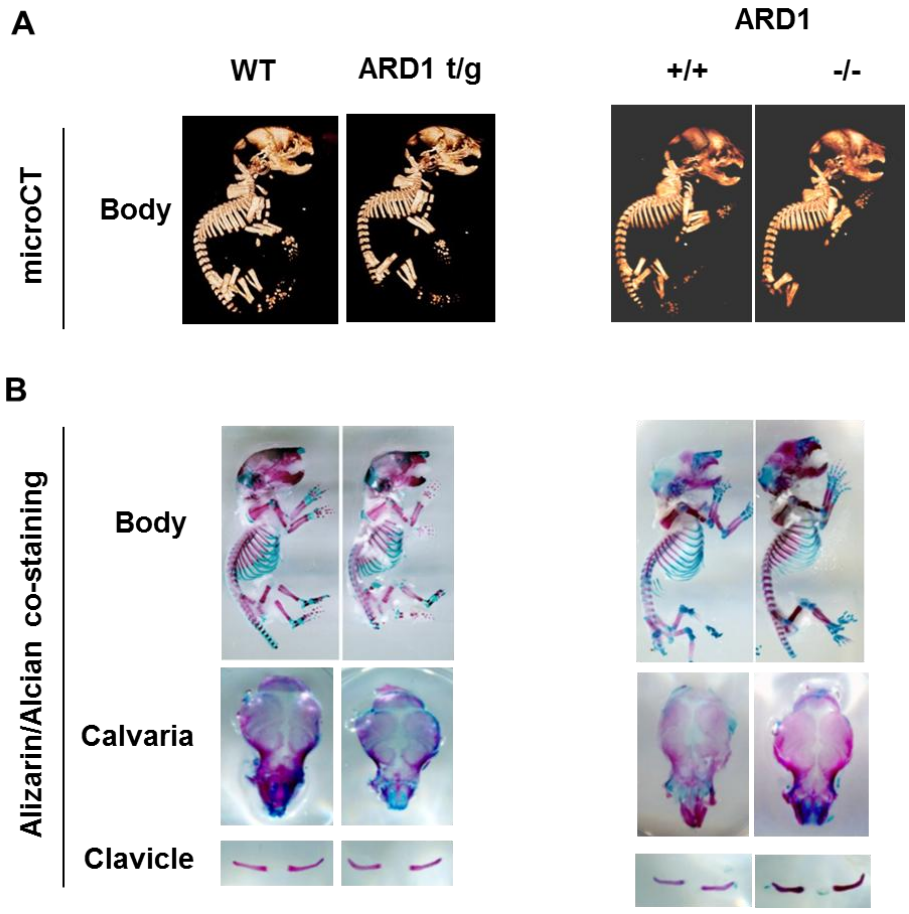
A
WT
ARD1 t/g
ARD1
+/+
-/-
microCT
Body
B
Alizarin/Alcian co-staining
Body
Calvaria
Clavicle

Figure 15. Skeletal structures of wild type, ARD1 transgenic mice, and ARD1 knock-out mice.

(A) Representative microCT images of mouse whole bodies. (B) Mice at a postnatal 3 day were stained with Alcian blue and Alizarin red. Calvarias and clavicles were isolated and pictured separately.

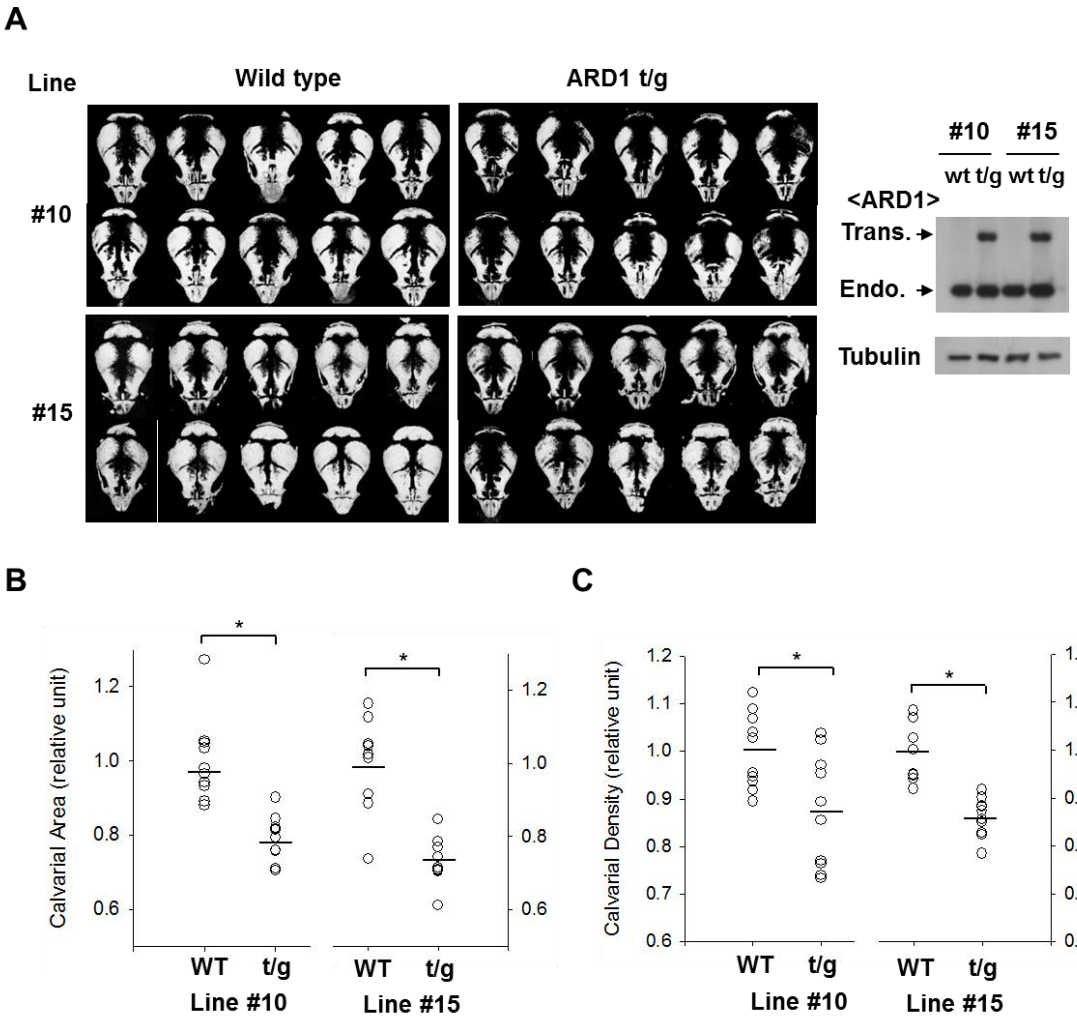
A
Line
Wild type
ARD1 t/g
#10
#15
#10 #15
wt t/g wt t/g
<ARD1>
Trans.
Endo.
Tubulin
B
Calvarial Area (relative unit)
1.2
1.0
0.8
0.6
*
*
WT t/g
Line #10
WT t/g
Line #15
C
Calvarial Density (relative unit)
1.2
1.1
1.0
0.9
0.8
0.7
0.6
*
*
WT t/g
Line #10
WT t/g
Line #15

Figure 16. Calvarial bone development is delayed in ARD1 transgenic mice.

(A) Micro-CT images of calvarias were taken from two lines (#10 and #15) of ARD1 transgenic mice and their littermate mice at postnatal 3 day. In each line, 10 transgenic mice and 10 littermate mice were examined. All images were captured at the same magnification, and the representative images are shown. Expression of endogenous and ectopic ARD1 in calvarias of ARD1 transgenic mouse line #10 and #15 and their littermates. The lysates were isolated from calvaria and analyzed using immunoblotting with anti-ARD1 and β-tubulin (right panel). (B, C) Calvaria area and bone density were analyzed in wild-type and ARD1 transgenic mice using ImageJ densitometry program.. Short horizontal bars represent group mean values and * denotes $P<0.05$ between two groups.

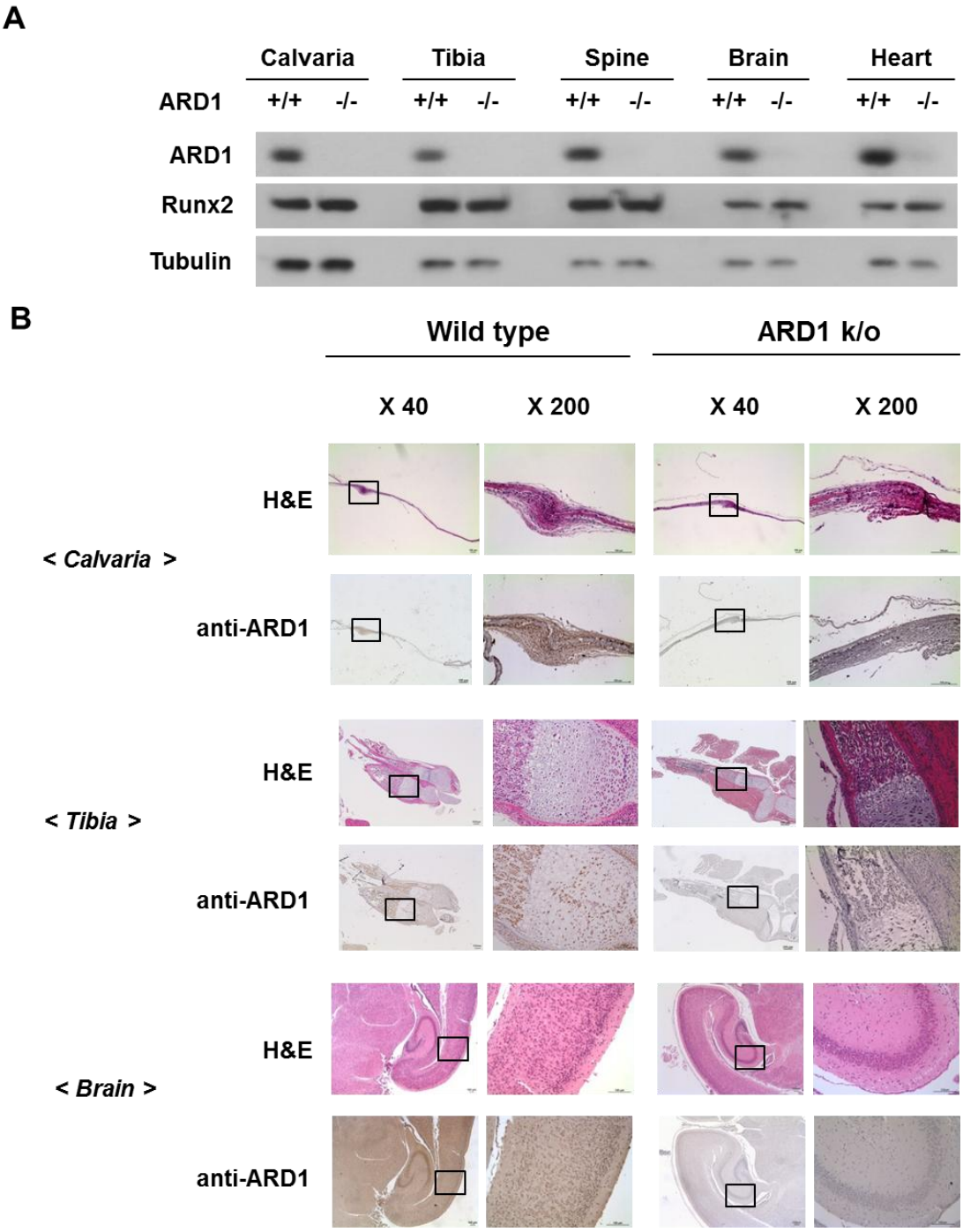
A
Calvaria
Tibia
Spine
Brain
Heart
ARD1 +/+ -/- +/+ -/- +/+ -/- +/+ -/- +/+ -/-
ARD1
Runx2
Tubulin
B
Wild type
ARD1 k/o
X 40
X 200
X 40
X 200
H&E
< Calvaria >
anti-ARD1
H&E
< Tibia >
anti-ARD1
H&E
< Brain >
anti-ARD1

Figure 17. ARD1 expressions in wild type and ARD1 knock-out mice.

(A) ARD1 and Runx2 levels were analyzed in various tissues form wild type ($ARD1^{+/+}$) and ARD1 knock-out ($ARD1^{-/-}$) mice by Western blotting. (B) Immunohistochemical analyses of ARD1 in $ARD1^{+/+}$ and $ARD1^{-/-}$ mouse. Paraffin tissue sections of mice at a postnatal 3 day were subjected to H&E staining and immunohistochemical analysis using anti-ARD1 antibody. Scale bar = 100 μm.

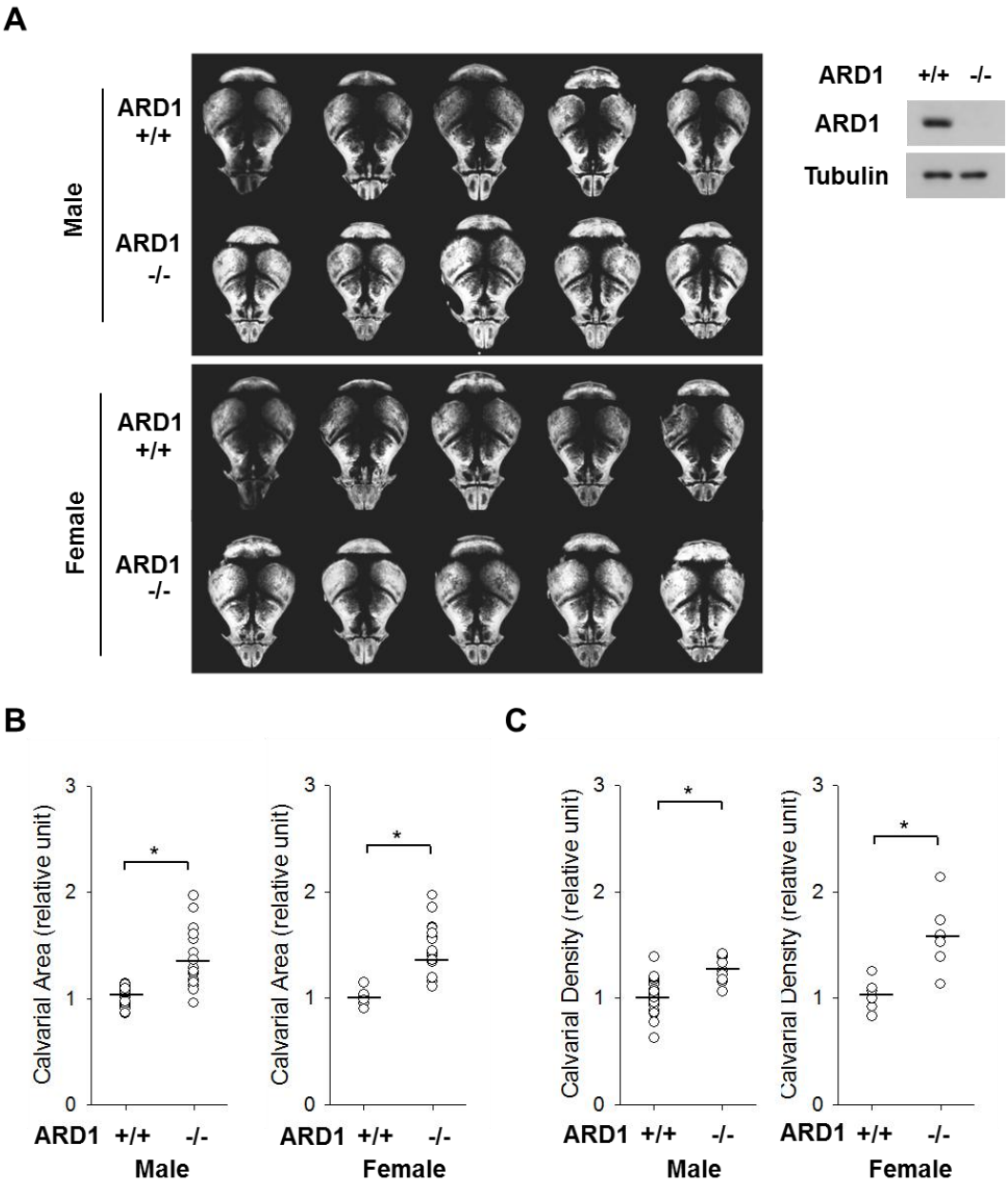
A
Male
ARD1 +/+
ARD1 -/-
Female
ARD1 +/+
ARD1 -/-
ARD1 +/+ -/-
ARD1
Tubulin
B
Calvarial Area (relative unit)
ARD1 +/+ -/-
Male
Calvarial Area (relative unit)
ARD1 +/+ -/-
Female
C
Calvarial Density (relative unit)
ARD1 +/+ -/-
Male
Calvarial Density (relative unit)
ARD1 +/+ -/-
Female

Figure 18. C**alvarial bone development is facilitated in ARD1 knock-out mice.**

(A) Micro-CT images of calvarias were taken from $ARD1^{+/+}$ (wt) and $ARD1^{-/-}$ mouse on postnatal day 3. All images were captured at the same magnification, and the representative images are shown. Male and female group were separately analyzed. ARD1 and β-tubulin levels were analyzed in the calvarias of $ARD1^{+/+}$ and $ARD1^{-/-}$ mice by Western blotting (right panel). (B, C) Calvarial area and bone density in $ARD1^{+/+}$ and $ARD1^{-/-}$ mouse were analyzed using ImageJ densitometry program. Short horizontal bars represent group mean values and * denotes $P<0.05$ between two groups.

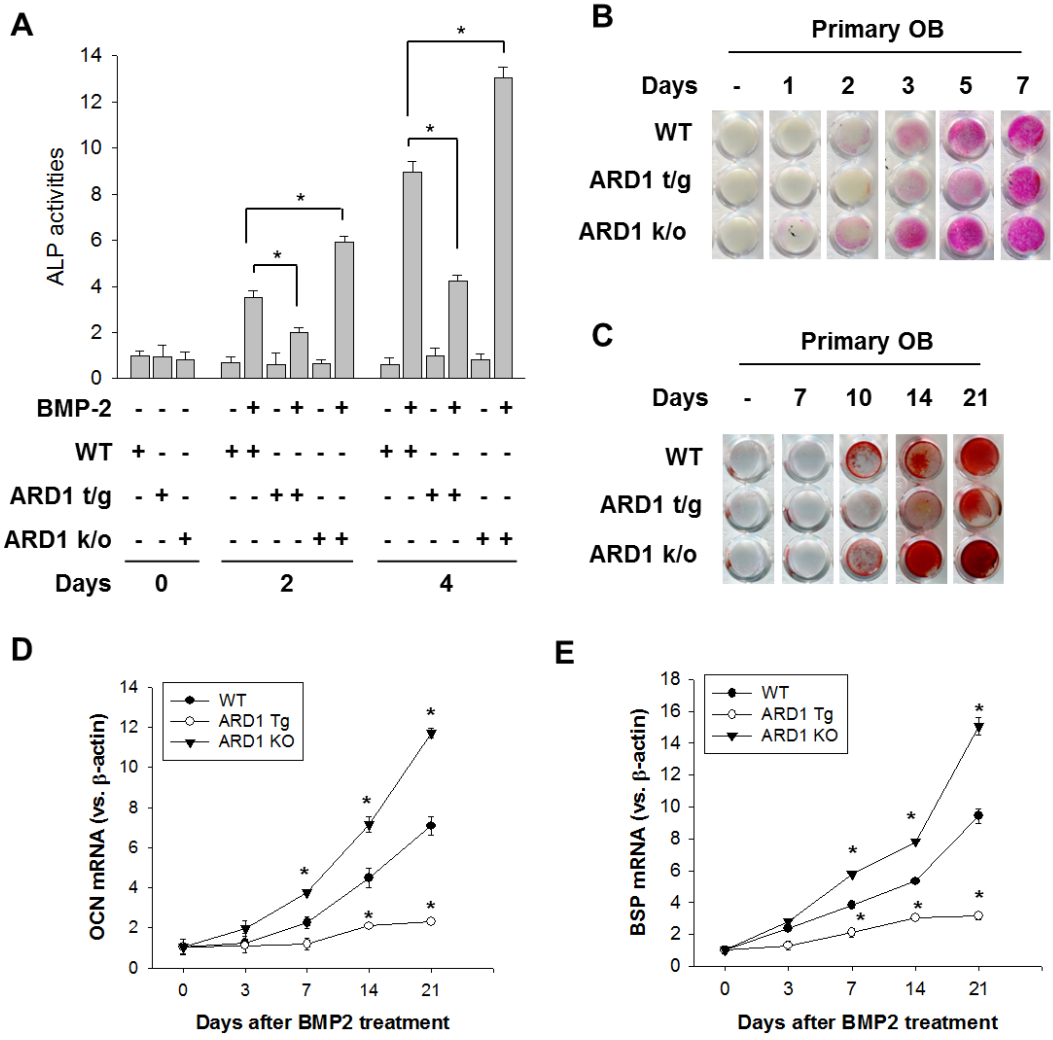
A
ALP activities
BMP-2
WT
ARD1 t/g
ARD1 k/o
Days
B
Primary OB
Days
WT
ARD1 t/g
ARD1 k/o
C
Primary OB
Days
WT
ARD1 t/g
ARD1 k/o
D
OCN mRNA (vs. β-actin)
WT
ARD1 Tg
ARD1 KO
Days after BMP2 treatment
E
BSP mRNA (vs. β-actin)
WT
ARD1 Tg
ARD1 KO
Days after BMP2 treatment

Figure 19. ARD1 inhibits osteoblast differentiation in primary osteoblasts from wild type, ARD1 transgenic mice and ARD1 knock-out mice.

(A) Primary osteoblasts from the indicated mice were incubated under PBS or BMP-2 for 2 or 4 days. ALP activities (means±SDs, n=4) were presented as relative values versus those of the PBS-treated WT mice. Primary osteoblasts were stained with ALP (B) and Alizarin Red S (C). The mRNA levels of OCN (D) and BSP (E) were quantified in primary osteoblasts by RT-qPCR. Results (means±SDs, n=4) are expressed as relative values versus the zero time control. * denotes $P<0.05$ versus the WT control.

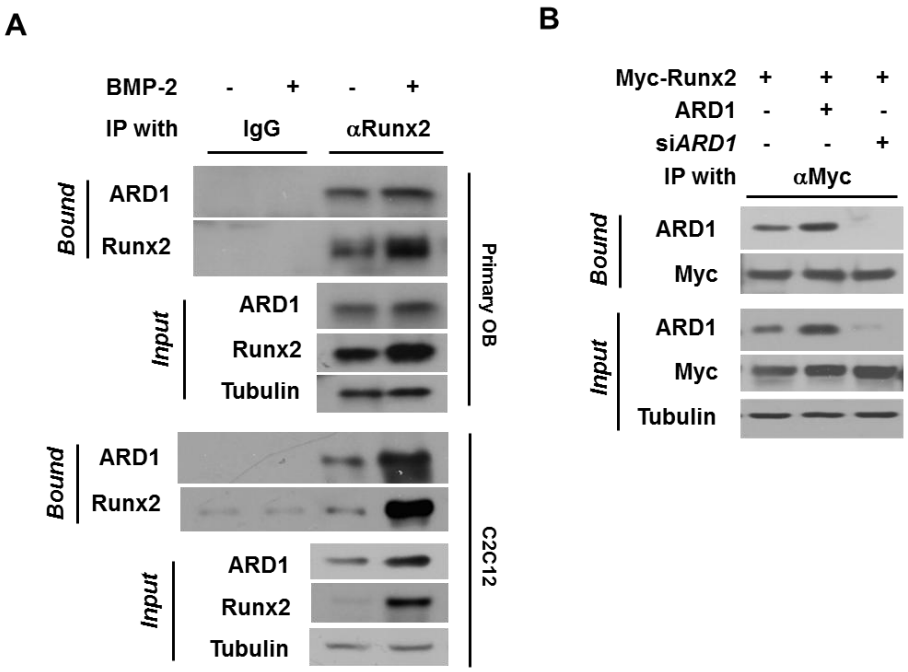
A
BMP-2 - + - +
IP with IgG αRunx2
Bound
ARD1
Runx2
Input
ARD1
Runx2
Tubulin
Primary OB
Bound
ARD1
Runx2
Input
ARD1
Runx2
Tubulin
C2C12
B
Myc-Runx2 + + +
ARD1 - + -
siARD1 - - +
IP with αMyc
Bound
ARD1
Myc
Input
ARD1
Myc
Tubulin

Figure 20. ARD1 interacts with Runx2.

(A) Primary osteoblast cells and C2C12 cells were treated with BMP-2 at 100 ng/ml for 4 days. Cell extracts were then immunoprecipitated with anti-Runx2, and precipitated Runx2 and ARD1 were immunoblotted with specific antibodies. (B) Myc-Runx2 plasmid was co-transfected with ARD1 plasmid or its siRNA into HEK293T cells. The interaction between Myc-Runx2 and ARD1 was identified by immunoprecipitation using anti-Myc and by immunoblotting with anti-ARD1.

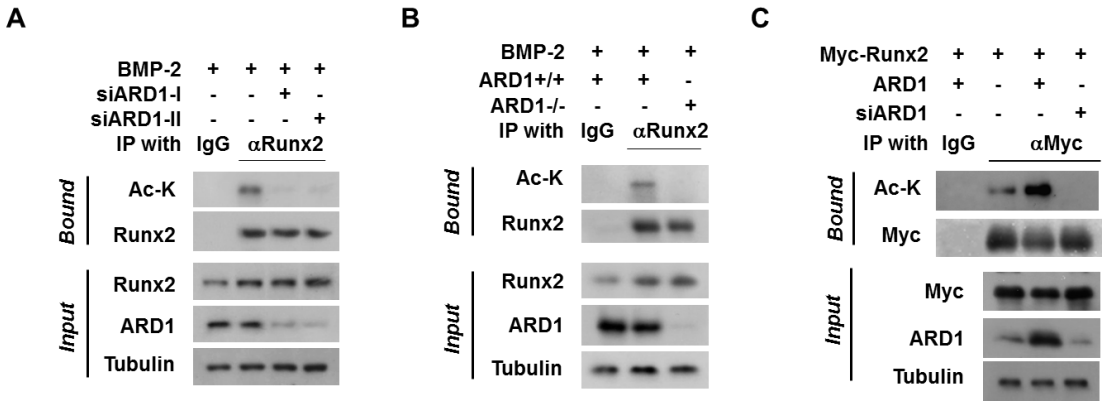
A
BMP-2 + + + +
siARD1-I - - + -
siARD1-II - - - +
IP with IgG αRunx2
Bound
Ac-K
Runx2
Input
Runx2
ARD1
Tubulin
B
BMP-2 + + +
ARD1+/+ + + -
ARD1-/- - - +
IP with IgG αRunx2
Bound
Ac-K
Runx2
Input
Runx2
ARD1
Tubulin
C
Myc-Runx2 + + + +
ARD1 + - + -
siARD1 - - - +
IP with IgG αMyc
Bound
Ac-K
Myc
Input
Myc
ARD1
Tubulin

Figure 21. ARD1 directly binds and acetylates Runx2.

(A) Primary osteoblast cells were transfected with ARD1-targeted siRNAs and treated with BMP-2 at 100 ng/ml for 4 days. After then, the cells were incubated with 1 μM Trichostatin A (a deacetylase inhibitor) for 6 hours. Cell extracts were then immunoprecipitated with anti-Runx2, and its acetylation was analyzed by Western blotting using an anti-acetyl lysine antibody. (B) Primary osteoblasts from wild type and ARD1 knock-out mice were treated with BMP-2 for 4 days. After being incubated with 1 μM Trichostatin A for 6 hours, cells were subjected to immunoprecipitation with anti-Runx2, and Runx2 acetylation was analyzed using anti-acetyl lysine antibody. (C) Myc-Runx2 plasmid was co-transfected with ARD1 plasmid or siRNA into HEK293T cells. Cells were treated with 1 μM Trichostatin A (a deacetylase inhibitor) for 6 hours and then lysed. Myc-Runx2 was precipitated using anti-Myc and its acetylation was analyzed by Western blotting using anti-acetyl lysine antibody.

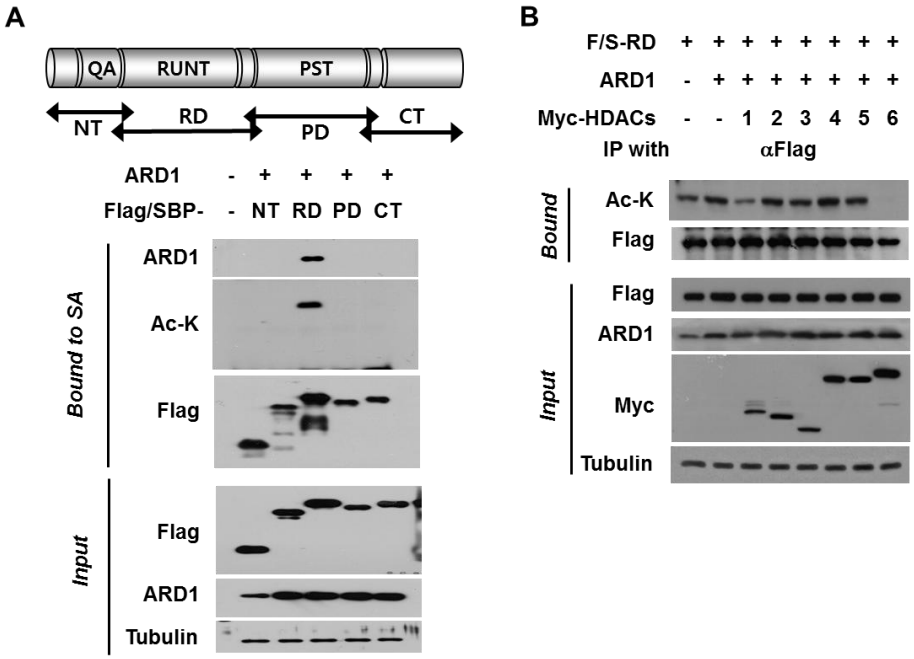
A
QA
RUNT
PST
NT
RD
PD
CT
ARD1 - + + + +
Flag/SBP- - NT RD PD CT
Bound to SA
ARD1
Ac-K
Flag
Input
Flag
ARD1
Tubulin
B
F/S-RD + + + + + + + +
ARD1 - + + + + + + +
Myc-HDACs - - 1 2 3 4 5 6
IP with αFlag
Bound
Ac-K
Flag
Input
Flag
ARD1
Myc
Tubulin

Figure 22. ARD1 binds and acetylates the RUNT domain of Runx2.

(A) Flag/SBP-tagged Runx2 constructs are illustrated in the top panel. HEK293T cells were co-transfected with plasmids of a Runx2 peptide and ARD1, and treated with Trichostatin A for 6 hours. Flag/SBP-peptides were pulled-down with streptoavidin-affinity beads, and ARD1 co-precipitation and lysyl acetylation were analyzed by Western blotting. (B) HEK293T cells were co-transfected with plasmids of Flag/SBP-RD, ARD1 and Myc-HDACs, and then treated with Trichostatin A for 6 hours. Flag/SBP-RD peptide was pulled-down using Flag-affinity beads, and the lysyl acetylation of RD peptide was analyzed by Western blotting.

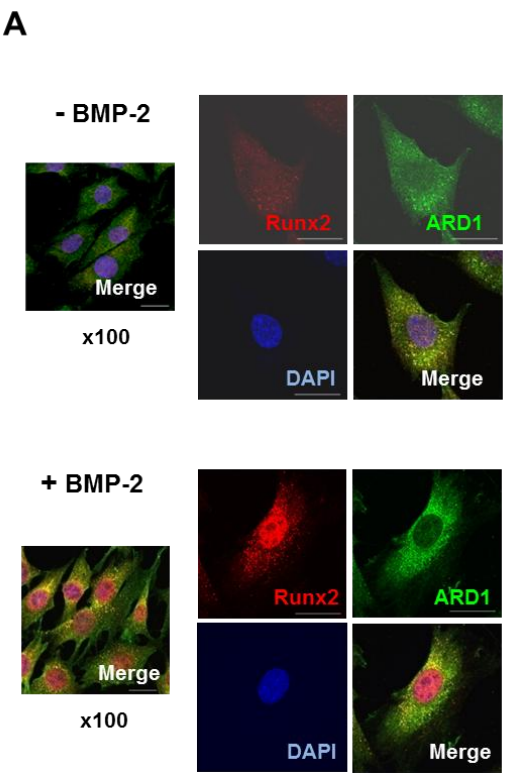
A
- BMP-2
Merge
x100
Runx2
ARD1
DAPI
Merge
+ BMP-2
Merge
x100
Runx2
ARD1
DAPI
Merge

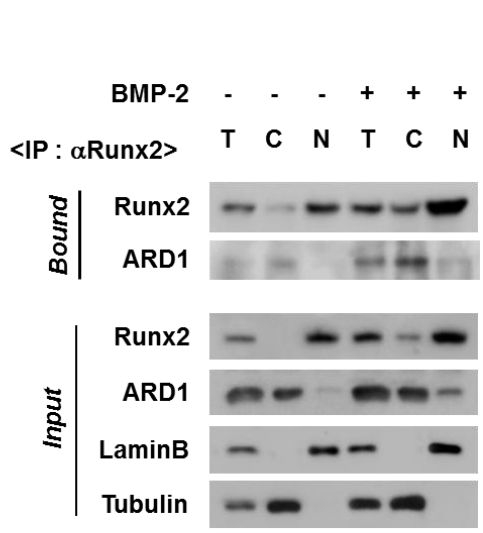
B
BMP-2 - - - + + +
<IP : αRunx2> T C N T C N
Bound
Runx2
ARD1
Input
Runx2
ARD1
LaminB
Tubulin

Figure 23. ARD1 binds and acetylates Runx2 in cytosol.

(A) Primary osteoblasts were treated with PBS or BMP-2, and subjected to immunocytochemical analyses with anti-Runx2 or anti-ARD1 antibody. The sections were visualized at 568 nm for Runx2 or at 488 nm for ARD1 under OLYMPUS fluorescence microscope. Scale bar, 20 μm. (B) Primary osteoblasts were lysed and fractionated into total (T), cytosolic (C) and nuclear (N) components. The cellular fractions were immunoprecipitated with anti-Runx2, and the precipitates were analyzed by Western blotting using indicated antibodies.

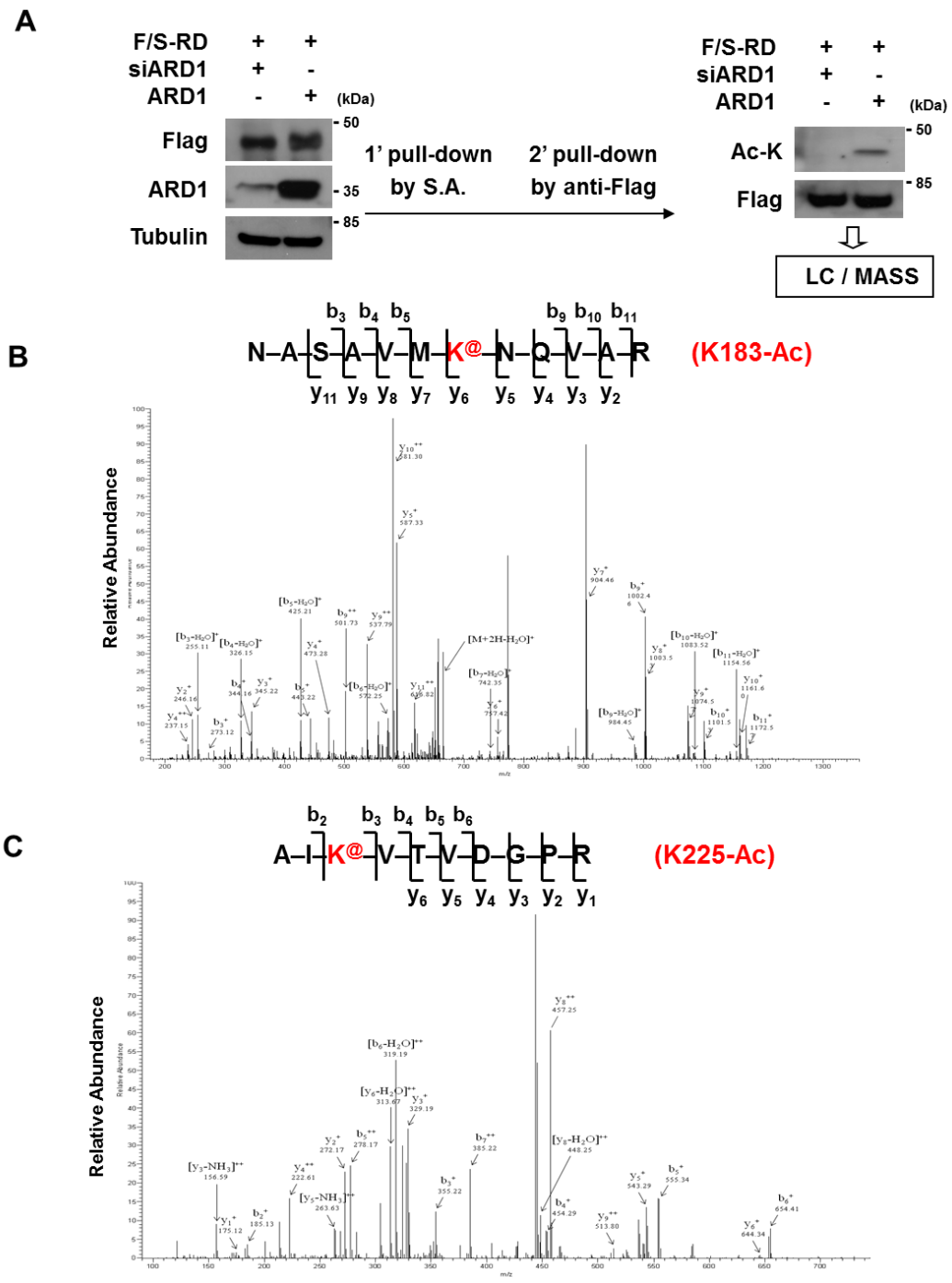
A
F/S-RD + +
siARD1 + -
ARD1 - +
(kDa)
Flag
ARD1
Tubulin
50
35
85
1' pull-down by S.A.
2' pull-down by anti-Flag
Ac-K
Flag
LC / MASS
B
N–A–S–A–V–M–K@–N–Q–V–A–R
(K183-Ac)
Relative Abundance
C
A–I–K@–V–T–V–D–G–P–R
(K225-Ac)
Relative Abundance

Figure 24. Runx2 is identified to be acetylated at K183 and K225.

HEK293T cells were co-transfected with Flag/SBP-RD and ARD1 plasmid. Cells were lysed and Flag/SBP-RD peptide was isolated through two-step affinity chromatography using SA and Flag affinity beads. Isolated Flag/SBP-RD peptide was run on SDS-PAGE, and subjected to an in-gel trypsin digestion (A). The LC/MS spectra detecting K183 acetylation and K225 are shown in (B) and (C) panels, respectively. Acetylation is indicated by an additional mass of 42 Daltons.

A

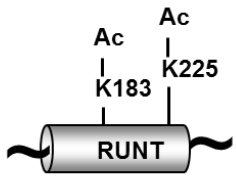

	183	225
Mouse:	LRNASAVM**K**NQVARFN	VATYHRAI**K**VTVDGPRE
Human:	LRNASAVM**K**NQVARFN	VATYHRAI**K**VTVDGPRE
Chicken:	LRNASAVM**K**NQVARFN	VATYHRAI**K**VTVDGPRE
Xenopus:	LRNASAVM**K**NQVARFN	VATYHRAI**K**VTVDGPRE

B

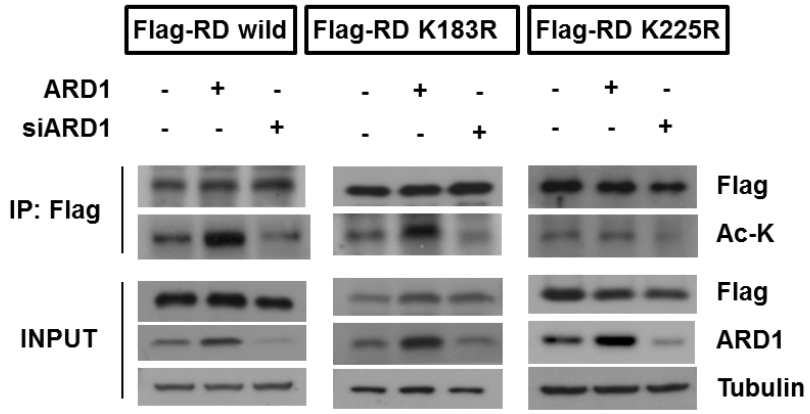

Figure 25. ARD1 acetylates K225 at RUNT of Runx2.

(A) Lysine residues 183 and 225 are well conserved among different species. (B) Flag/SBP-RD, Flag/SBP-RD K183R, or Flag/SBP-RD K225R plasmids were co-transfected with ARD1 plasmid or siRNA into HEK293T cells. After treated with 1 μM Trichostatin A, cells were lysed and incubated with anti-Flag and Flag/SBP-RD peptides and their lysyl-acetylations were analyzed by Western blotting.

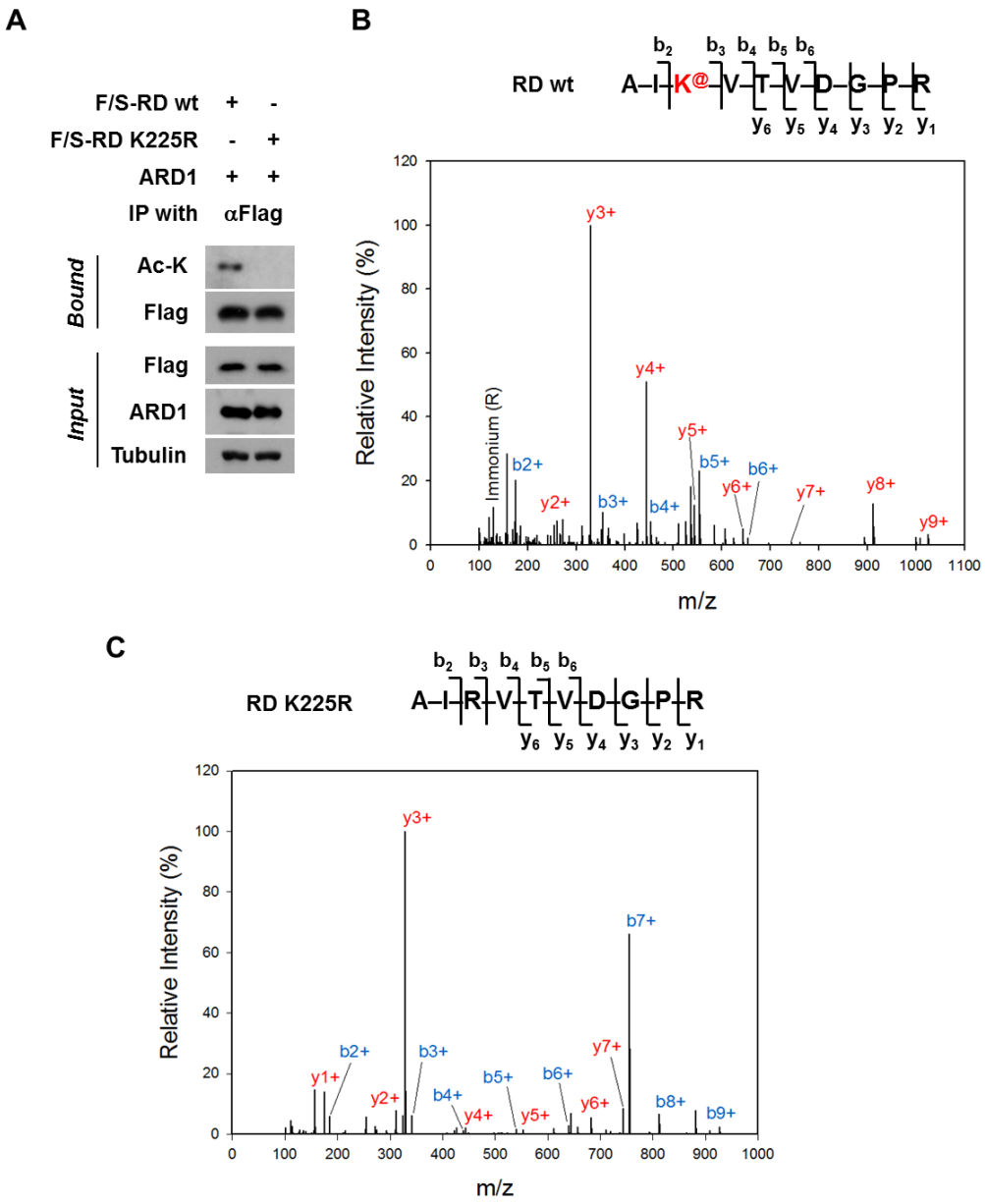
A
F/S-RD wt + -
F/S-RD K225R - +
ARD1 + +
IP with αFlag
Bound
Ac-K
Flag
Input
Flag
ARD1
Tubulin
B
RD wt
A–I–K@–V–T–V–D–G–P–R
Relative Intensity (%)
m/z
Immonium (R)
y3+
y4+
y5+
b2+
b5+
b6+
y6+
y7+
y8+
y2+
b3+
b4+
y9+
C
RD K225R
A–I–R–V–T–V–D–G–P–R
Relative Intensity (%)
m/z
y3+
b7+
b2+
b3+
y7+
y1+
y2+
b4+
b5+
b6+
y4+
y5+
y6+
b8+
b9+

Figure 26. ARD1 acetylates mouse Runx2 at K225.

HEK293T cells were co-transfected with ARD1 plasmid, Flag/SBP-RD or Flag/SBP-RD K225R. Flag/SBP-tagged peptides were purified using anti-Flag affinity beads, run on SDS-PAGE, and analyzed acetylation (A). The LC/MS spectra of WT and K225R-mutated peptides are shown in (B) and (C) panels, respectively.

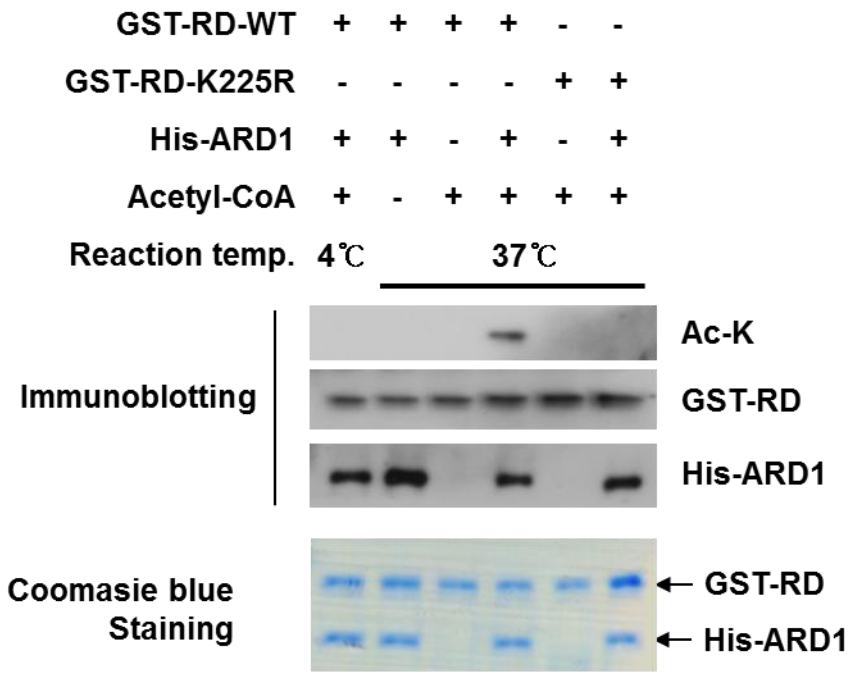
GST-RD-WT + + + + - -
GST-RD-K225R - - - - + +
His-ARD1 + + - + - +
Acetyl-CoA + - + + + +
Reaction temp. 4℃ 37℃
Immunoblotting
Ac-K
GST-RD
His-ARD1
Coomasie blue Staining
GST-RD
His-ARD1

Figure 27. ARD1 acetylates Runx2 at Lys 225 *in vitro*.

Recombinant His-ARD1 and GST-Runt (or its K225R mutant) peptides were incubated in the acetyl-CoA-containing reaction mixture for protein acetylation at 4^{o}C or 37^{o}C for 4 hours. The acetylation of GST-Runt peptides was identified using anti-acetyl-lysine antibody. The peptides on a gel were stained with Coommasie blue (bottom panel).

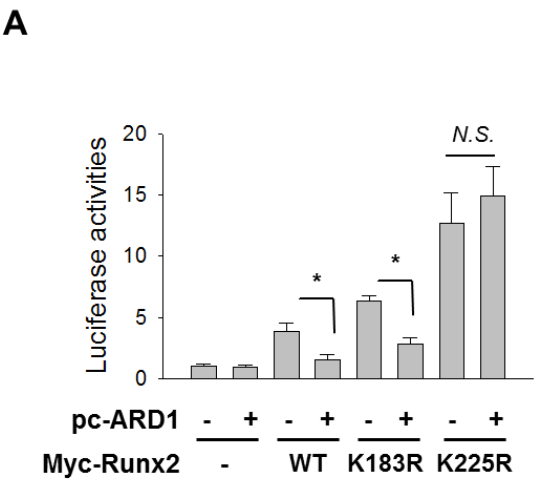
A
Luciferase activities
20
15
10
5
0
N.S.
*
*
pc-ARD1 - + - + - + - +
Myc-Runx2 - WT K183R K225R

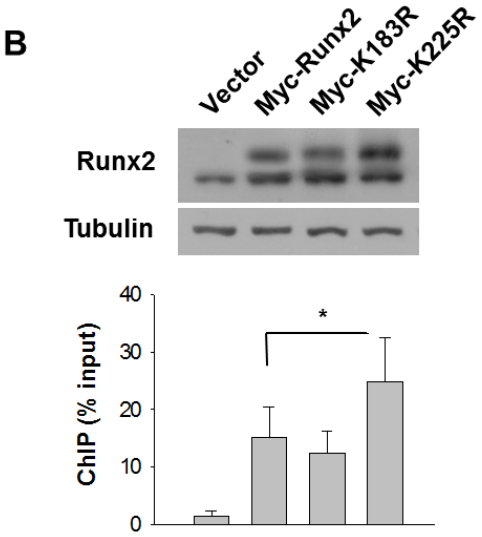
B
Vector
Myc-Runx2
Myc-K183R
Myc-K225R
Runx2
Tubulin
ChIP (% input)
40
30
20
10
0
*

Figure 28. ARD1 inhibits the transcriptional activity of Runx2 by acetylating it at K225.

(A) C2C12 cells were co-transfected with OG2-luciferase, β-gal, a Myc-Runx2 (full-length), Myc-Runx2 K183R, and Myc-Runx2 K225R plasmids. Luciferase activities (means±SD, n=4) were normalized versus β-gal activities and are presented relative to ARD1(-) and Runx2(-) values. (B) C2C12 cells, which had been transfected with one of the indicated plasmids, were treated with BMP-2 for 48 hours and Runx2 levels were checked by Western blotting (top). Cells were fixed with formalin and cross-linked chromatins were immunoprecipitated with anti-Runx2. DNAs were eluted and real-time PCR was performed to amplify the mouse osteocalcin (OCN) promoter region. * denotes $P<0.05$ between two groups.

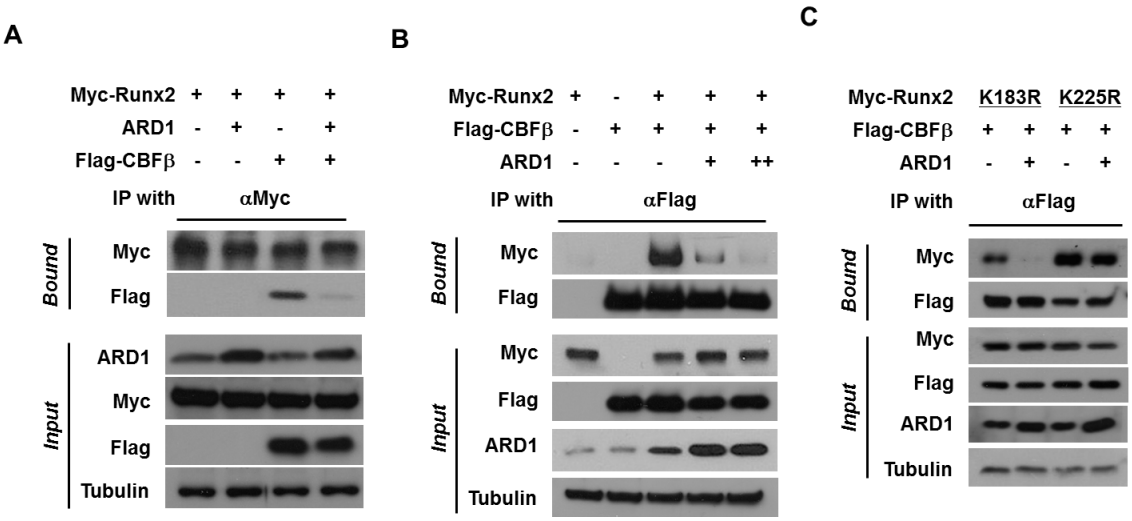
A
Myc-Runx2 + + + +
ARD1 - + - +
Flag-CBFβ - - + +
IP with αMyc
Bound
Myc
Flag
Input
ARD1
Myc
Flag
Tubulin
B
Myc-Runx2 + - + + +
Flag-CBFβ - + + + +
ARD1 - - - + ++
IP with αFlag
Bound
Myc
Flag
Input
Myc
Flag
ARD1
Tubulin
C
Myc-Runx2 K183R K225R
Flag-CBFβ + + + +
ARD1 - + - +
IP with αFlag
Bound
Myc
Flag
Input
Myc
Flag
ARD1
Tubulin

Figure 29. ARD1 blocks the Runx2-CBFβ interaction by acetylating Runx2 at K225.

(A) HEK293T cells were co-transfected with Myc-Runx2, ARD1, and Flag-CBFβ plasmids. Myc-Runx2 was precipitated with anti-Myc, and co-precipitated Flag-CBFβ was analyzed using anti-Flag. (B) In HEK293 cells transfected with 2 or 4 μg of ARD1, Flag-CBFβ precipitated with anti-Flag and co-precipitated Myc-Runx2 was analyzed using anti-Myc. (C) In HEK293 cells transfected with Myc-Runx2 K183R or Myc-Runx2 K225R plasmid, Flag-CBFβ was precipitated with anti-Flag and co-precipitated Myc-Runx2 mutants were analyzed using anti-Myc.

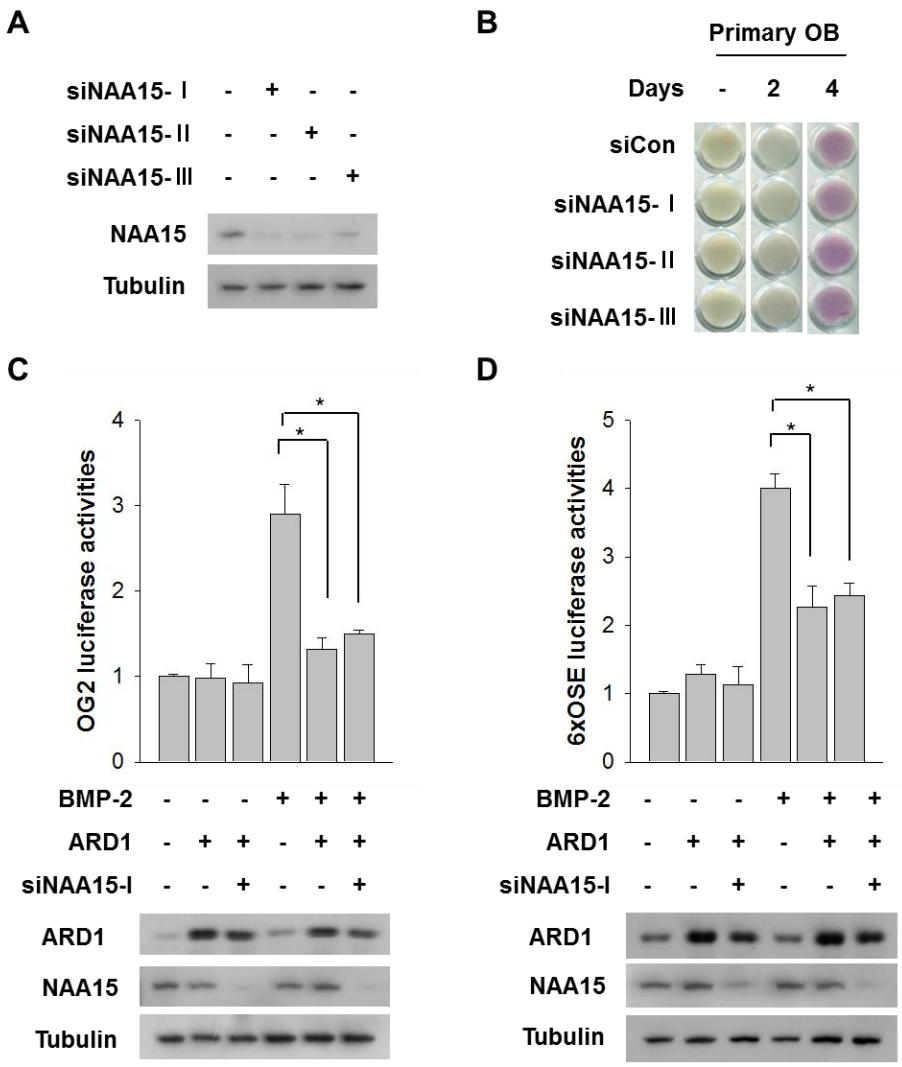
A
siNAA15-Ⅰ - + - -
siNAA15-Ⅱ - - + -
siNAA15-Ⅲ - - - +
NAA15
Tubulin
B
Primary OB
Days - 2 4
siCon
siNAA15-Ⅰ
siNAA15-Ⅱ
siNAA15-Ⅲ
C
OG2 luciferase activities
0 1 2 3 4
* *
BMP-2 - - - + + +
ARD1 - + + - + +
siNAA15-I - - + - - +
ARD1
NAA15
Tubulin
D
6xOSE luciferase activities
0 1 2 3 4 5
* *
BMP-2 - - - + + +
ARD1 - + + - + +
siNAA15-I - - + - - +
ARD1
NAA15
Tubulin

Figure 30. NAA15 is not required for the ARD1 inhibition of Runx2 during BMP-2-induced osteoblasts differentiation.

Primary osteoblasts, which had been transfected with Naa15-targeting siRNAs, were treated with BMP-2 for 2 or 4 days. NAA15 knock-down and osteoblast differentiation were evaluated using Western blotting (A) and ALP staining (B), respectively. OG2-luciferase plasmid (C) or 6XOSE-luciferase plasmid (D) was co-transfected with β-gal plasmid, ARD1 plasmid, and/or Naa15 siRNA into primary osteoblasts. After being stabilized for 48 hours, cells were treated with PBS or BMP-2 for 24 hours. Cells were lysed for reporter assays (top panel) or for Western blotting (bottom panel). Luciferase activities (means±SDs, n=4) were normalized versus β-gal activity, and are presented as relative values with respect to the vector controls. * denotes $P<0.05$.

GRAPHICAL SUMMARY

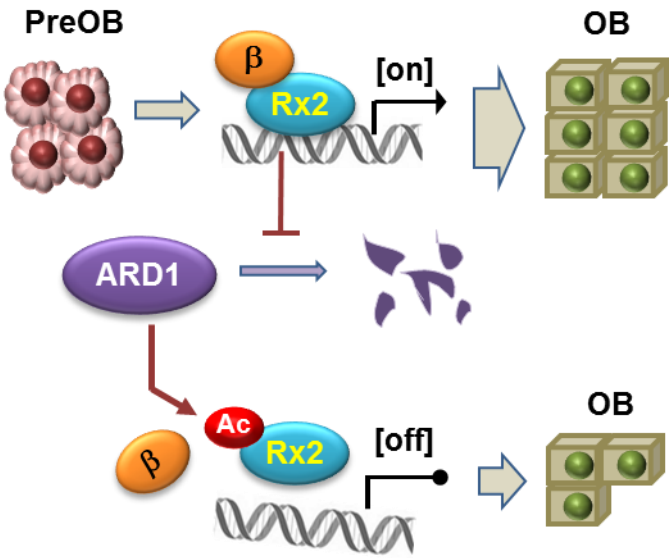

OB: osteoblast Rx2: Runx2 β: CBFβ
Ac: acetylation [ ]: transcriptional state

Figure 31. Proposed mechanism for the role of ARD1 in Runx2-mediated osteoblast differentiation.

DISCUSSION

This study demonstrates that ARD1 controls osteoblastogenesis by inhibiting Runx2 in a negative feed-back manner. Runx2 is a key molecule to modulate osteogenesis. Most of osteogenic factors, which are participated in osteoblast differentiation at early stage, are regulated by Runx2. Therefore, Runx2 activity must be fine-tuned during differentiation. The result presented here show that ARD1 is able to guard the balanced action of Runx2 during osteoblastogenesis. ARD1 protein is stabilized by BMP-2 induced Runx2. On the contrary, ARD1 disturbs the interaction of Runx2 with CBFβ as a result of acetylation of Runx2 at Lys225 and leads the repression of Runx2-driven transcription. Accordingly, ARD1 represses BMP-2-induced osteoblastogenesis (Fig. 34). Therefore, based on this scenario, it was performed that ARD1 was knock-downed in defective rat skulls and obtained successfully bone healing.

Yeast ARD1 was originally found to be essential for cell growth and sporulation (Whiteway et al., 1985; Mullen et al., 1989). ARD1 orthologs have been identified in most of mammalian species, including humans. ARD1 modulates cell fate using its enzymatic activity of the N-terminal α-acetylation at proteins in yeast and mammalian cells. ARD1 is known to control the hypoxic signaling pathway by degradation of HIF-1α in mice (Jeong et al., 2002), as well as promote cell proliferation by activating β-

catenin in human lung cancer (Lim et al., 2006). In the case of human fibrosarcoma, ARD1 is able to regulate cell migration by inactivating myosin light chain kinase (Shin et al., 2009), and neuronal differentiation in mouse brain (Ohkawa et al., 2008; Sugiura et al., 2003). Much is known about ARD1, but less well understood. Most of mammalian proteins show N-terminal acetylation and some proteins must be required acetylation for their own function. ARD1 is ubiquitously expressed and regulates various aspects of cellular function by acetylating variety target genes in mammalian cells, suggesting that it must have more diverse functions rather than known. Given the results, I found a new function for ARD1 in osteoblastogenesis, and I provide a potential means of improving bone healing based on the targeting of ARD1.

In general, ARD1 is known as the catalytic subunit of NatA that acetylates the α-amino group in nascent peptides (Liszczak et al., 2013). In the NatA complex, ARD1 is heterodimerized with Nα-acetyltransferase 15 (NAA15). ARD1 can catalyze N-terminal α-acetylation or lysine ε-acetylation in many proteins as post-translational modification (Jeong et al., 2002; Lim et al., 2006; Shin et al., 2009; Wang et al., 2012; Van et al., 2011). Moreover, without NAA15, ARD1 has its enzymatic activity as a monomer. However, a previous study demonstrated that NAA15 associated with Ku70 and Ku80 promote the Runx2-driven transcription of the OCN gene in osteoblasts (Willis et al., 2002). Therefore, it was examined whether NAA15 is involved in the ARD1 regulation of Runx2, but found that NAA15 is not required for

such an action of ARD1 (Fig. 30). ARD1 seems to be a solo player that controls osteoblast differentiation by acetylating Runx2 at K225.

Cellular components of the skeleton are composed of osteoblasts, chondrocytes, and myoblasts, which derived from mesenchymal stem cells. Differentiation and regulation of these cell fates are determined by key transcription factors such as Runx2, Osterix, and canonical Wnt signaling pathways (Komori., 2006). Moreover, these factors interplay between each other to proceed with differentiation to immature osteoblast. Runx2 acts a regulator in early stage of differentiation, contrary, is inhibitor in later osteoblast maturation. For example, it was reported that Runx2 transgenic mice showed severe osteopenia with multiple fractures and depressed osteoblast osteocalcin levels (Geoffroy et al., 2002). These findings suggest that Runx2 suppresses osteoblast maturation during late differentiation. The result presented here show that ARD1 inhibition augments osteoblast differentiation by activating Runx2. Regarding of inhibitory effect of Runx2 at late osteoblast stage, it appears that the depletion of ARD1 accelerates osteoblastogenesis during the early stage. Consistent with these observations, it was found that the depletion of ARD1 promotes osteoblast maturation by analyzing of osteocalcin, BSP, mineralization, and *in vivo* bone formation. These strongly suggest that ARD1 is involved in osteoblast maturation.

To date, two types of orthologs of Runx2 have been uncovered type I of Runx2 is strongly expession in pre-osteoblast and chondrocyte precursor cells. While, type II is expressed in matured osteoblasts and terminal

chondrogenesis (Park et al., 2001; Sato et al., 2008). Out data presented here shows that the bone formation in calvaria area was retarded in ARD1 transgenic mice, because Runx2 transcriptional activity was suppressed. But, there appeared to be no change in the length of femur and tibia, and formation, which must be modulated by chondrocyte differentiation. Therefore, ARD1 represses osteoblast differentiation through inhibition of transcriptional activity at type II of Runx2 rather than type I.

During early stage of osteoblastogenesis, the expression levels of Runx2 and ARD1 were increased but IKKβ was decreased. Moreover, it was found that Runx2 induces ARD1 by inhibiting the IKKβ-mediated destabilization of ARD1. Under inflammatory conditions, when IKKβ phosphorylates and destabilizes IκBα, NF-κB enters into the nucleus and expresses a variety of proinflammatory genes. Likewise, IKKβ has been known to phosphorylate many proteins other than IκBα and to inhibit their functions. For instance, the substrates of IKKβ include IRS1, DOK1, FOXO3a, and TSC1. Recently, ARD1 was also demonstrated to be destabilized through IKKβ-mediated phosphorylation (Kuo et al., 2009). I here found that Runx2 suppresses the action of IKKβ during osteoblastogenesis. However, the underlying molecular mechanism about the downregulation of Runx2 onto IKKβ remains to be elucidated. Given that Runx2 is a transcription factor, I propose that Runx2 promotes the expression of IKKβ-degrading proteins like Keap1 or it acts as a repressor of the IKKβ gene (Lee et al., 2012).

Runx2 has been known to recruit histone acetyltransferases (HATs) such as CBP, p300, P/CAF, MOZ, and MORF and so on. Usually, HATs disentangle tight chromatins to help Runx2 access DNA, and it becomes undergo to enhance Runx2-driven transcription (Bae et al., 2006). Furthermore, p300 has been reported to stabilize and activate Runx2 by directly acetylating Runx2 (Jeon et al., 2006). Although the lysine residues for acetylation were not identified by mass analysis, mutational studies suggested that mouse Runx2 is acetylated at multiple residues including K225, K230, K350, and K351. However, it was insufficiency to explain how Runx2 activity is regulated by being acetylated at each lysine residue. Unlikely p300, ARD1 repressed the transcriptional function of Runx2 by the acetylation onto K225 residue, while it would not influence the stability of Runx2. Furthermore, acetylation at K225 of Runx2 can interfere the binding with CBFβ. Interestingly, it appears that both p300 and ARD1 acetylate Runx2, but regulate Runx2 activity in the opposite manners, which is activated by p300 and repressed by ARD1. The functional consequences of Runx2 acetylation may be determined by the acetylation on specific residue. Taken together, when p300 is constantly expressed, p300 supports Runx2 activation during the initial stages of osteoblast differentiation. After then, to do not excessive function of Runx2, ARD1 controls negatively Runx2 which is activated by p300 at the next step of differentiation. However, this hypothesis remains to be elucidated.

CBFβ is a co-activator essential for the activation of Runx families.

Although it does not bind to DNA directly, CBFβ enhances the DNA binding capability of Runx proteins and activates Runx-driven transcription (Blyth et al., 2005). Indeed, it has been demonstrated that CBFβ is required for Runx2-dependent bone development during the embryonic and postnatal stages (Kundu et al., 2002; Kanatani et al., 2006). In the present study, it was found that the ARD1-mediated K225 acetylation of Runx2 blocks CBFβ binding to Runx2. This acetylation may change the confirmation of RUNT domain to a form unfavorable for CBFβ binding. Given the role of CBFβ suggested previously, the dissociation of CBFβ from acetylated Runx2 do not explain why ARD1 reduces the DNA binding ability of Runx2. However, as the Runt domain directly binds to DNA, it is also possible that the acetyl moiety carries a negative charge, and it becomes RUNT acetylation disrupts interaction with DNA to Runx2. However, this possibility also remains to be investigated.

BMPs are a subfamily of the TGF-β superfamily and have several subgroups by sequence homology. BMPs are secreted by osteoblasts and chondrocytes and stimulate their differentiations. Furthermore, BMPs bind to serine/threonine kinase receptors in progenitor cells and induce the phosphorylations of Smads. After then, smads enter the nucleus and express involved skeletal formation genes and other transcription factors (Hirata et al., 2010; Massague et al., 2005). Given the role of BMPs, recombinant human BMP-2 and BMP-7 have been clinical tested to promote bone healing in open fractures. Nowadays, the collagen matrix containing recombinant BMPs have

been utilized to treat within fracture area, and several similar products have been approved by US Food and Drug Administration (McKay et al., 2007). A number of prospective studies have shown that the implantation of recombinant BMP-2 or BMP-7 significantly increases union rates and shortens times to union (Govender et al., 2002; Giannoudis et al., 2005). In the present study, BMP-2 in collagen matrix was also implanted into 8-mm sized calvarial defects, which are too large to recover spontaneously, and it was found that BMP-2 can induce new bone formation. However, it was also found that the depletion of an ARD1 can activate more BMP-2-induced bone formation. Accordingly, this study suggests that ARD1 inhibition offers a potential means of improving BMPs-dependent fracture healing. Nevertheless, small-molecules inhibiting ARD1 would be more relevant to clinical applications than the shRNA virus used in this mechanism study, but they have not been identified so far.

Summarizing, this study shows that Runx2 stabilizes ARD1 and that ARD1 inhibits Runx2. This negative feed-back loop definitely modulates the Runx2 signaling pathway and maintains balance between Runx2 and other osteogenic factors. Perhaps, the constrained inhibition of ARD1 could result in loose bone due to the premature termination of osteoblastogenesis. However, once fractured bone has been fixed, loose bone is usually replaced by hard bone through bone remodeling. For the early rehabilitation of patients with open fracture required early fixation is first considered. Accordingly, this study proposes that ARD1 inhibition is to be considered as a new strategy to

aid fracture healing. Also, loss-of-function mutations in human Runx2 lead to bone disease like as cleidocranial dysplasia (CCD). CCD is a skeletal and dental disorder caused by week bone formation. Taken together, this study suggests that ARD1 inhibition is a new target for healing Runx2-dependent hereditary disease.

REFERENCES

1. Arnesen T, Anderson D, Baldersheim C, Lanotte M, Varhaug JE, Lillehaug JR. Identification and characterization of the human ARD1-NATH protein acetyltransferase complex. Biochem J. 2005 Mar 15;386(Pt 3):433-43.
2. Arnesen T, Van Damme P, Polevoda B, Helsens K, Evjenth R, Colaert N, et al. Proteomics analyses reveal the evolutionary conservation and divergence of N-terminal acetyltransferases from yeast and humans. Proc Natl Acad Sci U S A. 2009 May 19;106(20):8157-62.
3. Bae SC, Lee YH. Phosphorylation, acetylation and ubiquitination: the molecular basis of RUNX regulation. Gene. 2006 Jan 17;366(1):58-66.
4. Blyth K, Cameron ER, Neil JC. The RUNX genes: gain or loss of function in cancer. Nat Rev Cancer. 2005 May;5(5):376-87.
5. Cameron ER, Neil JC. The Runx genes: lineage-specific oncogenes and tumor suppressors. Oncogene. 2004 May 24;23(24):4308-14.
6. Chan HM, La Thangue NB. p300/CBP proteins: HATs for transcriptional bridges and scaffolds. J Cell Sci. 2001 Jul;114(Pt 13):2363-73.
7. Choi JY, Pratap J, Javed A, Zaidi SK, Xing L, Balint E, et al. Subnuclear targeting of Runx/Cbfa/AML factors is essential for tissue-specific differentiation during embryonic development. Proc Natl Acad Sci U S A. 2001 Jul 17;98(15):8650-5.
8. Ducy P, Zhang R, Geoffroy V, Ridall AL, Karsenty G. Osf2/Cbfa1: a transcriptional activator of osteoblast differentiation. Cell. 1997 May 30;89(5):747-54.
9. Franceschi RT, Ge C, Xiao G, Roca H, Jiang D. Transcriptional regulation of osteoblasts. Ann N Y Acad Sci. 2007 Nov;1116:196-207.
10. Fisher TS, Etages SD, Hayes L, Crimin K, Li B. Analysis of ARD1 function in hypoxia response using retroviral RNA interference. J Biol

Chem. 2005 May 6;280(18):17749-57.

11. Geoffroy V, Kneissel M, Fournier B, Boyde A, Matthias P. High bone resorption in adult aging transgenic mice overexpressing cbfa1/runx2 in cells of the osteoblastic lineage. Mol Cell Biol. 2002 Sep;22(17):6222-33.
12. Giannoudis PV, Tzioupis C. Clinical applications of BMP-7: the UK perspective. Injury. 2005 Nov;36 Suppl 3:S47-50.
13. Govender S, Csimma C, Genant HK, Valentin-Opran A, Amit Y, Arbel R, et al. Recombinant human bone morphogenetic protein-2 for treatment of open tibial fractures: a prospective, controlled, randomized study of four hundred and fifty patients. J Bone Joint Surg Am. 2002 Dec;84-A(12):2123-34.
14. Hirata S, Kitamura C, Fukushima H, Nakamichi I, Abiko Y, Terashita M, et al. Low-level laser irradiation enhances BMP-induced osteoblast differentiation by stimulating the BMP/Smad signaling pathway. J Cell Biochem. 2010 Dec 15;111(6):1445-52.
15. Ito Y. Oncogenic potential of the RUNX gene family: 'overview'. Oncogene. 2004 May 24;23(24):4198-208.
16. Jeong JW, Bae MK, Ahn MY, Kim SH, Sohn TK, Bae MH, et al. Regulation and destabilization of HIF-1alpha by ARD1-mediated acetylation. Cell. 2002 Nov 27;111(5):709-20.
17. Jeon EJ, Lee KY, Choi NS, Lee MH, Kim HN, Jin YH, et al. Bone morphogenetic protein-2 stimulates Runx2 acetylation. J Biol Chem. 2006 Jun 16;281(24):16502-11.
18. Jonason JH, Xiao G, Zhang M, Xing L, Chen D. Post-translational Regulation of Runx2 in Bone and Cartilage. J Dent Res. 2009 Aug;88(8):693-703.
19. Jun JH, Yoon WJ, Seo SB, Woo KM, Kim GS, Ryoo HM, et al. BMP2-activated Erk/MAP kinase stabilizes Runx2 by increasing p300 levels and histone acetyltransferase activity. J Biol Chem. 2010 Nov 19;285(47):36410-9.

20. Kalvik TV, Arnesen T. Protein N-terminal acetyltransferases in cancer. Oncogene. 2013 Jan 17;32(3):269-76.
21. Kanatani N, Fujita T, Fukuyama R, Liu W, Yoshida CA, Moriishi T, et al. Cbf beta regulates Runx2 function isoform-dependently in postnatal bone development. Dev Biol. 2006 Aug 1;296(1):48-61.
22. Komori T. Regulation of osteoblast differentiation by transcription factors. J Cell Biochem. 2006 Dec 1;99(5):1233-9.
23. Komori T. Regulation of bone development and extracellular matrix protein genes by RUNX2. Cell Tissue Res. 2010 Jan;339(1):189-95.
24. Komori T. Signaling networks in RUNX2-dependent bone development. J Cell Biochem. 2011 Mar;112(3):750-5.
25. Kouzarides T. Acetylation: a regulatory modification to rival phosphorylation? The EMBO journal. 2000 Mar 15;19(6):1176-9.
26. Kundu M, Javed A, Jeon JP, Horner A, Shum L, Eckhaus M, et al. Cbfbeta interacts with Runx2 and has a critical role in bone development. Nat Genet. 2002 Dec;32(4):639-44.
27. Kuo HP, Lee DF, Chen CT, Liu M, Chou CK, Lee HJ, et al. ARD1 stabilization of TSC2 suppresses tumorigenesis through the mTOR signaling pathway. Science signaling. 2010;3(108):ra9.
28. Kuo HP, Lee DF, Xia W, Lai CC, Li LY, Hung MC. Phosphorylation of ARD1 by IKKbeta contributes to its destabilization and degradation. Biochem Biophys Res Commun. 2009 Nov 6;389(1):156-61.
29. Lee KS, Kim HJ, Li QL, Chi XZ, Ueta C, Komori T, et al. Runx2 is a common target of transforming growth factor beta1 and bone morphogenetic protein 2, and cooperation between Runx2 and Smad5 induces osteoblast-specific gene expression in the pluripotent mesenchymal precursor cell line C2C12. Molecular and cellular biology. 2000 Dec;20(23):8783-92.
30. Lee MN, Lee SN, Kim SH, Kim B, Jung BK, Seo JH, et al. Roles of arrest-defective protein 1(225) and hypoxia-inducible factor 1alpha in

tumor growth and metastasis. J Natl Cancer Inst. 2010 Mar 17;102(6):426-42.

31. Lee SH, Che X, Jeong JH, Choi JY, Lee YJ, Lee YH, et al. Runx2 protein stabilizes hypoxia-inducible factor-1alpha through competition with von Hippel-Lindau protein (pVHL) and stimulates angiogenesis in growth plate hypertrophic chondrocytes. J Biol Chem. 2012 Apr 27;287(18):14760-71.
32. Li QL, Ito K, Sakakura C, Fukamachi H, Inoue K, Chi XZ, et al. Causal relationship between the loss of RUNX3 expression and gastric cancer. Cell. 2002 Apr 5;109(1):113-24.
33. Lim JH, Park JW, Chun YS. Human arrest defective 1 acetylates and activates beta-catenin, promoting lung cancer cell proliferation. Cancer Res. 2006 Nov 15;66(22):10677-82.
34. Liszczak G, Goldberg JM, Foyn H, Petersson EJ, Arnesen T, Marmorstein R. Molecular basis for N-terminal acetylation by the heterodimeric NatA complex. Nat Struct Mol Biol. 2013 Sep;20(9):1098-105.
35. Long F. Building strong bones: molecular regulation of the osteoblast lineage. Nat Rev Mol Cell Biol. 2011 Dec 22;13(1):27-38.
36. Massague J, Seoane J, Wotton D. Smad transcription factors. Genes Dev. 2005 Dec 1;19(23):2783-810.
37. McKay WF, Peckham SM, Badura JM. A comprehensive clinical review of recombinant human bone morphogenetic protein-2 (INFUSE Bone Graft). Int Orthop. 2007 Dec;31(6):729-34.
38. Monroe DG, McGee-Lawrence ME, Oursler MJ, Westendorf JJ. Update on Wnt signaling in bone cell biology and bone disease. Gene. 2012 Jan 15;492(1):1-18.
39. Mullen JR, Kayne PS, Moerschell RP, Tsunasawa S, Gribskov M, Colavito-Shepanski M, et al. Identification and characterization of genes and mutants for an N-terminal acetyltransferase from yeast. EMBO J. 1989 Jul;8(7):2067-75.

40. Nishimura R, Hata K, Matsubara T, Wakabayashi M, Yoneda T. Regulation of bone and cartilage development by network between BMP signalling and transcription factors. J Biochem. 2012 Mar;151(3):247-54.
41. Ohkawa N1, Sugisaki S, Tokunaga E, Fujitani K, Hayasaka T, Setou M, et al. N-acetyltransferase ARD1-NAT1 regulates neuronal dendritic development. Genes Cells. 2008 Nov;13(11):1171-83.
42. Okuda T, van Deursen J, Hiebert SW, Grosveld G, Downing JR. AML1, the target of multiple chromosomal translocations in human leukemia, is essential for normal fetal liver hematopoiesis. Cell. 1996 Jan 26;84(2):321-30.
43. Otto F, Thornell AP, Crompton T, Denzel A, Gilmour KC, Rosewell IR, et al. Cbfa1, a candidate gene for cleidocranial dysplasia syndrome, is essential for osteoblast differentiation and bone development. Cell. 1997 May 30;89(5):765-71.
44. Park MH, Shin HI, Choi JY, Nam SH, Kim YJ, Kim HJ, et al. Differential expression patterns of Runx2 isoforms in cranial suture morphogenesis. J Bone Miner Res. 2001 May;16(5):885-92.
45. Pelletier N, Champagne N, Stifani S, Yang XJ. MOZ and MORF histone acetyltransferases interact with the Runt-domain transcription factor Runx2. Oncogene. 2002 Apr 18;21(17):2729-40.
46. Pockwinse SM, Rajgopal A, Young DW, Mujeeb KA, Nickerson J, Javed A, et al. Microtubule-dependent nuclear-cytoplasmic shuttling of Runx2. J Cell Physiol. 2006 Feb;206(2):354-62.
47. Polevoda B, Sherman F. N-terminal acetyltransferases and sequence requirements for N-terminal acetylation of eukaryotic proteins. J Mol Biol. 2003 Jan 24;325(4):595-622.
48. Sato S, Kimura A, Ozdemir J, Asou Y, Miyazaki M, Jinno T, et al. The distinct role of the Runx proteins in chondrocyte differentiation and intervertebral disc degeneration: findings in murine models and in human disease. Arthritis Rheum. 2008 Sep;58(9):2764-75.

49. Schroeder TM, Jensen ED, Westendorf JJ. Runx2: a master organizer of gene transcription in developing and maturing osteoblasts. Birth Defects Res C Embryo Today. 2005 Sep;75(3):213-25.
50. Shin DH, Chun YS, Lee KH, Shin HW, Park JW. Arrest defective-1 controls tumor cell behavior by acetylating myosin light chain kinase. PLoS One. 2009 Oct 14;4(10):e7451.
51. Sierra J, Villagra A, Paredes R, Cruzat F, Gutierrez S, Javed A, et al. Regulation of the bone-specific osteocalcin gene by p300 requires Runx2/Cbfa1 and the vitamin D3 receptor but not p300 intrinsic histone acetyltransferase activity. Mol Cell Biol. 2003 May;23(9):3339-51.
52. Sugiura N, Adams SM, Corriveau RA. An evolutionarily conserved N-terminal acetyltransferase complex associated with neuronal development. J Biol Chem. 2003 Oct 10;278(41):40113-20.
53. Van Damme P, Evjenth R, Foyn H, Demeyer K, De Bock PJ, Lillehaug JR, et al. Proteome-derived peptide libraries allow detailed analysis of the substrate specificities of N(alpha)-acetyltransferases and point to hNaa10p as the post-translational actin N(alpha)-acetyltransferase. Mol Cell Proteomics. 2011 May;10(5):M110.004580.
54. Wang Z, Wang Z, Guo J, Li Y, Bavarva JH, Qian C, et al. Inactivation of androgen-induced regulator ARD1 inhibits androgen receptor acetylation and prostate tumorigenesis. Proc Natl Acad Sci U S A. 2012 Feb 21;109(8):3053-8.
55. Wee HJ, Huang G, Shigesada K, Ito Y. Serine phosphorylation of RUNX2 with novel potential functions as negative regulatory mechanisms. EMBO reports. 2002 Oct;3(10):967-74.
56. Whiteway M, Szostak JW. The ARD1 gene of yeast functions in the switch between the mitotic cell cycle and alternative developmental pathways. Cell. 1985 Dec;43(2 Pt 1):483-92.
57. Willis DM, Loewy AP, Charlton-Kachigian N, Shao JS, Ornitz DM, Towler DA. Regulation of osteocalcin gene expression by a novel Ku

antigen transcription factor complex. J Biol Chem. 2002 Oct 4;277(40):37280-91.

58. Xiao G, Jiang D, Gopalakrishnan R, Franceschi RT. Fibroblast growth factor 2 induction of the osteocalcin gene requires MAPK activity and phosphorylation of the osteoblast transcription factor, Cbfa1/Runx2. The Journal of biological chemistry. 2002 Sep 27;277(39):36181-7.
59. Zhang YW, Yasui N, Kakazu N, Abe T, Takada K, Imai S, et al. PEBP2alphaA/CBFA1 mutations in Japanese cleidocranial dysplasia patients. Gene. 2000 Feb 22;244(1-2):21-8.
60. Zhao M, Qiao M, Oyajobi BO, Mundy GR, Chen D. E3 ubiquitin ligase Smurf1 mediates core-binding factor alpha1/Runx2 degradation and plays a specific role in osteoblast differentiation. J Biol Chem. 2003 Jul 25;278(30):27939-44.

국문 초록

배경: 전사인자인 Runt-related transcription factor 2 (Runx2)는 골형성과 조골세포 분화에 관련된 많은 유전자들을 조절한다. Runx2는 단백질의 '번역후 수정 (post-translational modification)' 과정을 통해 단백질 안정성과 전사활성이 조절된다. Runx2의 '번역후 수정' 중 하나인 아세틸 수식은 Runx2의 전사활성 조절 중 알려진 유일한 원인이다. Runx2의 직접적인 아세틸 수식 인자로는 p300과 PCAF만이 알려져 있으나, 표적 잔기가 명확히 알려져 있지 않다. 한편, 아세틸화 효소인 arrest defective-1 (ARD1)은 효모에서 세포성장과 포자형성에 결정적인 역할을 하며, 포유류 암세포에서도 아미노산 lysine을 아세틸 수식하여 HIF-1α, β-catenin, MLCK등의 단백질 기능의 조절한다. 포유류 단백질 대부분이 아세틸 수식을 통해 단백질 기능과 안정성 조절을 받으며, 이를 ARD1이 조절할 것이라 예상한다. 하지만 뼈에서의 ARD1의 발생과 역할은 전혀 밝혀지지 않았다. 본 연구에서는 ARD1이 아세틸 수식을 통해 Runx2의 신호전달과 골 형성에서 역할을 연구하였다. **결과:** BMP-2의존적인 조골세포 분화 동안, ARD1과 Runx2의 단백질 수준이 함께 증가하였다. IKKβ는 ARD1의 serine 206 잔기를 인산화시켜 프로테아좀 분해시키는 것으로 알려진 효소이다. 조

골세포 분화 동안 Runx2는 IKKβ의 발현을 억제함으로써 ARD1의 단백질을 안정화시켰다. ARD1 억제 시 Runx2의 전사 활성이 촉진되어 조골세포 분화가 증가되었다. 이는 ARD1이 Runx2의 억제성 되먹임 조절자가 될 수 있음을 제시한다. 동물 모델에서, ARD1억제 시 쥐의 머리덮개 뼈의 결손 부분에서 골 재형성이 증가되었다. 또한, ARD1 형질전환 쥐에서 대조군에 비해 신생아 머리덮개 뼈의 골형성과 무기질 침착이 지연되었다. 반대로 ARD1 결손 쥐에서는 머리덮개 뼈의 골형성이 촉진되었다. ARD1 에 의한 골형성의 억제 기전은 다음과 같다. ARD1은 Runx2의 DNA 결합 영역으로 알려진 RUNT 영역의 lysine 225 잔기에 아세틸 수식을 했다. Runx2의 lysine 225의 아세틸 수식이 되면, Runx2의 전사 인자 도움 단백질로 알려진 CBFβ가 결합하지 못했다. 이를 통해 ARD1은 아세틸 수식을 통한 Runx2의 전사활성을 저해한다. 따라서 ARD1 억제제를 개발한다면, Runx2를 경유하는 골형성과 골재형성을 효과적으로 증가시킬 수 있을 것이다. **결론:** ARD1은 Runx2에 의해 조골세포 분화 과정 동안 단백질 안정성이 증가된다. ARD1은 Runx2의 억제성 되먹임 조절자로써 골 형성 기간 동안 Runx2의 전사 활성을 억제하여 조골세포 분화의 속도와 균형을 조절한다. 본 연구는 ARD1이 조골세포에서의 발현과 포유류 골형성에 중요함을 처음으

로 규명하였다. ARD1이 골형성과 치유에 관련된 골대사 질환의 새로운 치료 표적이 될 수 있음을 시사한다.

주요어: 조골세포 분화, ARD1, Runx2, 골 형성 단백질-2 (BMP-2)
학 번: 2011-30631